ANR escape

DELIVERABLE D3.3

Characterization of the observed and simulated historical climate variations at dekadal scales and interpretation in link with recent observations of the surface energy and water balance

Prepared by Françoise Guichard, with contributions from Laurent Kergoat, Frédéric Hourdin Eric Mougin and Dominique Bouniol

D3.3 a

Observed and simulated historical variations of surface thermodynamics at decadal scales

1. Introduction

The Sahel is perhaps the region on Earth which has experienced the largest climatic changes in the last decades. Multi-decadal fluctuations of rainfall, in particular the severe Sahelian droughts of the 70's and 80's have focused an important research activity since the pioneer studies of Lamb (1982), Hulme (1992), Hulme et al. (2001) among others - see Giannini (2008) for a review. The Sahel is also a region where temperature is extremely high in Spring, prior to the arrival of the monsoon rain; with for instance monthly mean temperature typically reaching 35°C at 15°N East of 10°W. Therefore, any climatic warming in Spring, as temperature is already at its annual maximum, is likely to have particularly strong societal implications. Observations show that the Sahelian region has experienced a strong warming since 1950. It is especially manifest in Spring (Fig. 1), and at night (see ESCAPE D1.1b), while multi-decadal fluctuations of monsoon rainfall shape more complex and coupled variations of temperature in summer, in particular the daily maximum temperature. On the other hand, multi-decadal variations in humidity have been found to be very complex to assess from observations and observational products (e.g. reanalyses) so far, for reasons previously discussed in ESCAPE deliverable D1.1b. Note that they are still the object of investigations within ESCAPE.

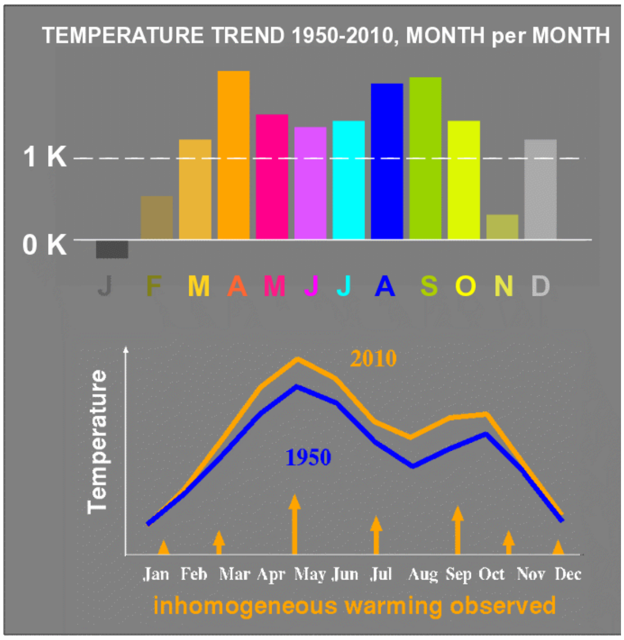

***Figure 1**: An illustration of the seasonal structure of the multi-decadal trend in surface temperature typically observed in the Sahel between 1950 and 2010.*

The data used here are the daily-mean surface temperature of the Hombori meteorological station (SYNOP observations).

The top panel shows the trend as a function of month of year and the bottom panel contrasts the seasonal cycle in 1950 and 2010, with a notable warming outside of the dry cool season, and especially in spring.

We are using these observations to explore the performance of recently released climate simulations part of the Coupled Model Intercomparison Project Phase 5 (CMIP5). Because the multi-decadal climatic fluctuations display a well defined annual cycle, and because of the predominance of the annual cycle in the Sahelian climate, we extensively study the simulations from this 'annual cycle' perspective.

Climate simulations are often inter-compared and assessed in terms of their respective climatic trends, regardless of their mean climate. At the same time, reasonable simulation of the present climate does not guaranty by itself the relevance of the climatic projections obtained with the same model. In practice, some features, some parameters of models are tuned with respect to present climate, and the relevance of these internal elements of the models in another climate are not all obvious. However, the scatter obtained among different climate projections are not disconnected from biases affecting the climate simulated with the same models (e.g. Christensen and Boberg 2012). Furthermore, the current level of performance of general circulation models in West Africa, which is still poor, calls for majors improvements of the simulation of the present climate in this region, as shown in Roehrig et al. (2013) and further emphasized by the results presented below (see also Guichard et al. 2012).

Hereafter, the methodology is briefly introduced. Then the differing annual structures of the simulated climatic changes in surface air temperature are discussed, and the simulation of the annual cycle of this variable in models are presented.

2. Methodology

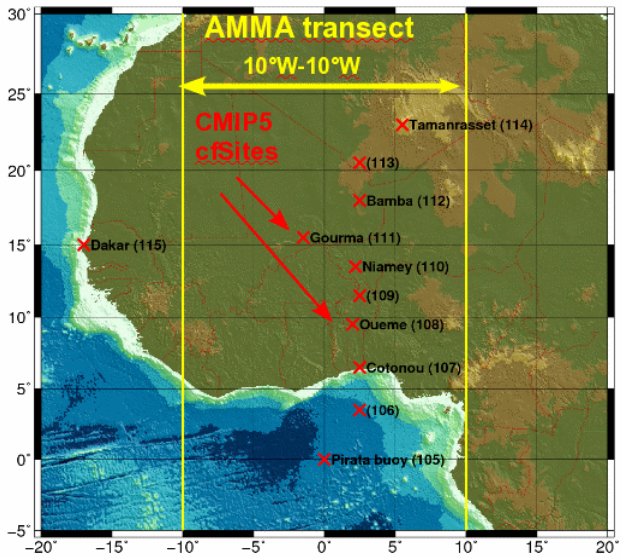

***Figure 2** : map of West Africa (orography) ; the two yellow lines delineate a meridional climatological transect (the AMMA transect); the eleven red crosses indicate locations where numerous high-frequency fields have been extracted from selected simulations, following a CFMIP proposal.*
(Source of figure: Dominique Bouniol)

In this study, the adopted methodology is driven by considerations of the meridional climatological gradient observed in West Africa, also adopted by Hourdin et al. (2010) in their evaluation of models over West Africa. Namely, they evaluated model performances focussing on the meridional structure of simulated fields averaged over [10°W,10°E] (Fig. 1, yellow lines).

Within the CFMIP project, which is coordinated with CMIP5, an ensemble of locations around the world were defined where modellers would provide more refined high-frequency simulated fields, refereed to as cfSites. This includes in particular the components of the surface energy budget components and atmospheric heat and water vapour budgets. Among these places, a chain of locations, indicated with red crosses in Fig. 2, was defined to sample the West African meridional gradient from the Gulf of Guinea to Tamanrasset in the Sahara (see also Dakar to the West). Several models have now provided high-frequency outputs for their amip simulations (corresponding to 30-year long simulations starting around 1980 and using prescribed SST).

This includes three simulations from ISPL, differing in their parametrizations or resolution, with IPSL-CM5a-LR using a standard configuration, IPSL-CM5b-LR a new set of physical parametrizations, and IPSL-CM5a-MR a refined grid (see Hourdin et al. 2013 a and b). This also includes a CNRM-CM5 simulation (Voldoire et al. 2013), together with two simulations from other European research centres (HadGEM2-a and EC-Earth), and three more from Canadian, Japanese and Chinese centres (CanAM4, MRI-CGCM3 and bcc-csm1-1).

The retrieval and manipulation of the large volume of generated cfSites files can be laborious, but so far, apart from the two last ones (MRI-CGCM3 and bcc-csm1-1), we have started to exploit all the other simulations. Note also that high-frequency typically means 30 min here, but a few models provided some simulated fields with a 3-h frequency instead. This concerns CNRM-CM5 for time varying fields, including the surface energy budget, EC-Earth for all fields, and HadGEM2-a for a few radiative fields. Not unexpected, we also noted a few mistakes in this huge amount of generated files. Keeping these informations in mind, the ensemble of files provide a great opportunity for in-depth physically-based evaluation of models, and potentially, valuable inference on their climatic projections.

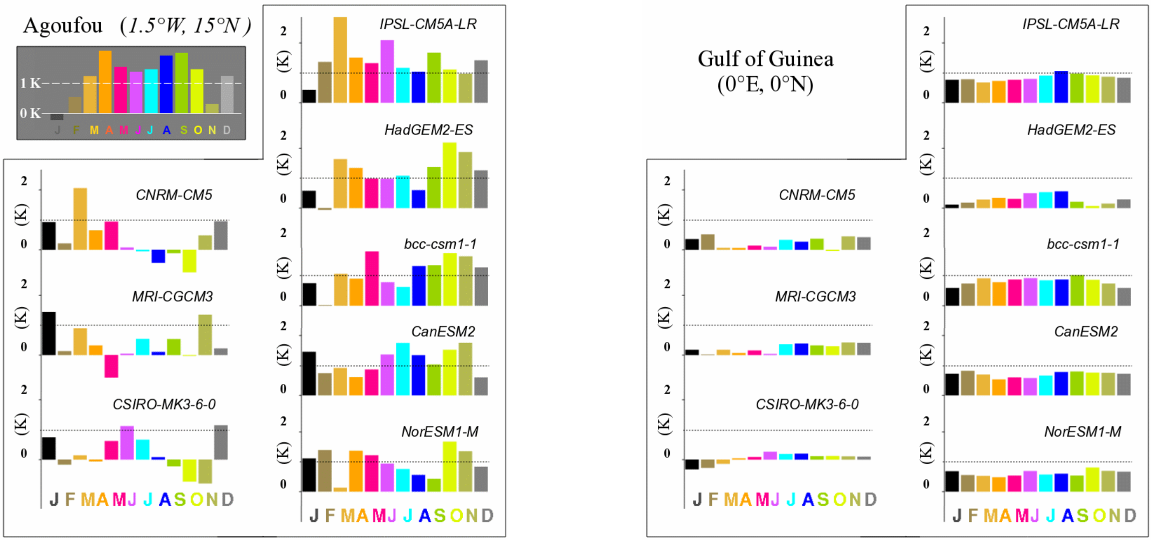

Figure 3: *Seasonal structure of the multi-decadal trend in surface temperature simulated between 1950 and 2010 with historical CMIP5 simulations at the closest point to Agoufou in central Sahel (left panel) and to 0°E0°N in the Gulf of Guinea. The names of the each model is given on each graph. In each panel, the models are group according to their weak (left column) or stronger (right) temperature trend. The upper left graph correspond to observations.*

In order to document the simulations of the multi-decadal trends over West Africa, we used historical and historicalNat simulations, as amip simulations start too late for this purpose. A West African zone was extracted from the CMIP5 files as well simulations outputs at location corresponding to the cfSites presented above. So far, we mostly used monthly-mean surface thermodynamic fields but plan to jointly analyse surface fluxes in the future. At the time when we started this work, less simulations were available, so that eight historical simulations are presented below. The historicalNat simulations were used to explore whether the trends obtained with the historical simulations departed from those obtained using natural forcing only.

Finally, we also incorporated results from some piControl simulations to explore more fully, for a given model, the sensitivity of the annual cycle structure to the configuration of the simulation.

3. Simulated multi-decadal trends in the annual cycle of surface air temperature

Multi-decadal trends of temperature in the historical and historicalNat simulations were analysed and determined in the same way as in observations (see ESCAPE D.1.1a, D1.1b), and the results were found to be zonally-consistent across the transect of Fig. 2. Figure 3 contrasts the difference in magnitude and seasonality of temperature trends simulated over the continental location of Central Sahel and in the Gulf of Guinea. There the trend is smaller, and it also displays much less fluctuations from month to month. The models characterized by a smaller trend over sea similarly display a smaller, underestimated trend over land. However, the annual structures of the simulated trends can be quite different from one model to the next and the models characterized by the smaller trends in historical simulations display trends of similar magnitude in historicalNat.

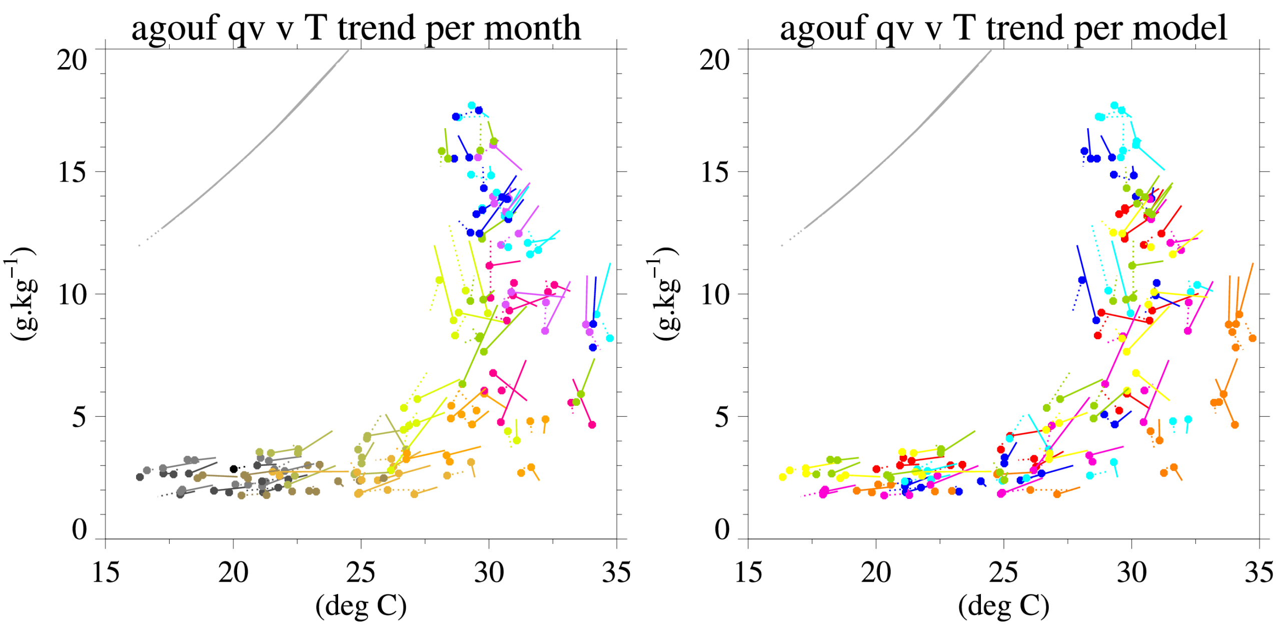

Figure 4: Scatter diagrams of monthly-mean qv versus T. Dots correspond to the initial values in 1950 given by the linear trend, it is linked by a line to the final values, solid (dotted) lines correspond to historical (historicalNat) simulations. The colour code in left (right) panel identify months (models). The curve in the upper left of the graphs coincides with saturation.

An analysis of the trends in other variable using the same annual cycle framework is not directly informative (see figure in Appendix A), partly because of major differences in the mean annual cycle among models as presented in next section. The trend in nocturnal temperature is generally more pronounced in models though, and coupled with a negative trend of DTR outside of the monsoon months.

This annual cycle issue can be already be guessed from the scatter diagrams linking T, qv and they respective trends, for historical and historicalNat simulations (Fig. 4). The larger trends are typically obtained during the spring and autumn months, and these are also the months for which the spread among model mean values are the stronger (orange and red colours in Fig. 4, left panel). Overall, positive trends are generally coupled with an increase in specific humidity whose magnitude also considerably varies among models. As a result, trends in relative humidity are found to be either positive or negative, and they are strongly coupled to trends in precipitation during the summer months (not shown).

4. Evaluation of the simulated annual cycle of temperature

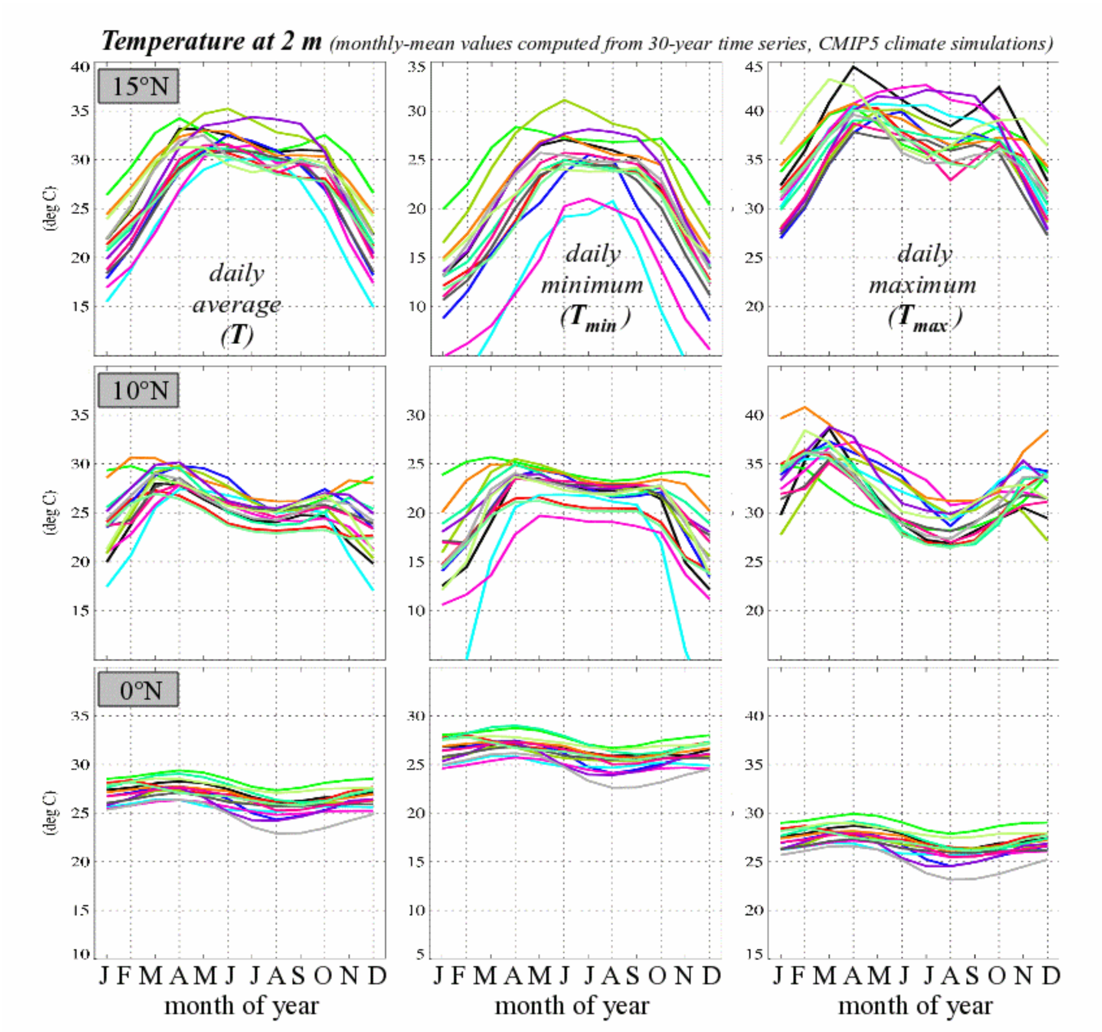

__Figure 5__: The annual cycle of temperature (left), Tmin (middle) and Tmax(right) presented with monthly-mean values (30-year average), from 0°E,0°N (bottom) to 15°N,0°E (top). Each colour identifies one model.

As we are more specifically interested in climatic changes occurring in spring, we analysed in more depth the simulated annual cycles of the temperature. Fig. 5 shows them as annual series of monthly-mean temperature, Tmin and Tmax at three different latitudes, from 0°N in the Gulf of Guinea to Central Sahel. As the climate become more continental and arid, it is notable that the spread among models increases, notably outside of the monsoon season (consistently with Fig. 4). During these months, it is also much larger for Tmin than Tmax. Conversely, the differences in Tmax can be more pronounced during the monsoon. Note that for a given model, the structure of the simulated annual cycle is very similar from one configuration to the other (amip, historical, piControl), and differences among models dominate over differences in configurations.

In D1.1.b, we emphasized the distinct annual cycle of Tmin and Tmax. The annual maximum of Tmax is indeed found to occur earlier than Tmin in most models as in observations. The simulated patterns are more or less shifted and pronounced, but some model totally miss this basic feature of the annual cycle, such as GISS-E2-R (not shown). The different nature of the processes shaping the evolution of Tmax and Tmin during the year probably account for their distinct annual structures, and multi-decadal trends. It seems that compensating errors between Tmin and Tmax fluctuations lead to slightly less spread in daily average temperature compared to Tmin and Tmax (Fig. 5, left panels). This diurnal sensitivity is further illustrated with series of monthly-mean diurnal cycles of temperature (cfSites outputs) together with data in Fig. 6. Here, data should be considered as indicative (they do not correspond to a climatic mean and variability from site to site is expected at small scale). However, the results point to distinct sources of biases from winter tiime, when simulated nighttime temperatures drops too much, to summer time, when conversely, daytime temperature rises too much in the same models.

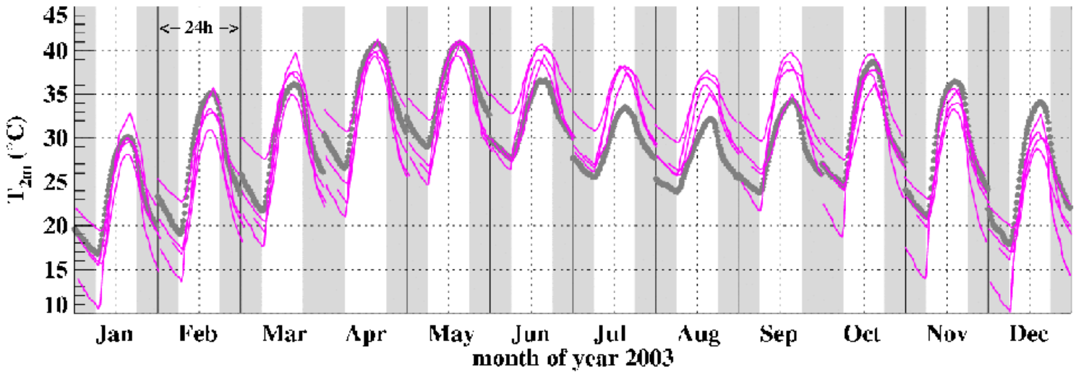

***Figure 6**: Monthly-mean diurnal cycle of temperature, simulated at the Gourma cfSite (pink) and observed at Agoufou (black).*

5. Summary

This study provides an evaluation of the annual structure of the multi-decadal trend in surface air temperature simulated by CMIP5 climate simulations, following a previous analysis of this trend in data (ESCAPE D1.1.a, D1.1.b), and with a particular focus on spring temperature. It appears that it is very challenging for models to reproduce this annual structure. This issue can be partly linked to the differing annual cycles upon which these trends arises in models, and to the different nature of the processes which are shaping the nighttime and daytime temperatures and warming trends throughout the year.

We are currently analysing cfSites fields to analyse the sources of these differences. Regarding nighttime temperature, it seems that the fine-scale vertical structure of the nocturnal boundary layer could account for some of the differences noted among models. More broadly, we are planning to pursue this analysis of model spread with a special focus on the DTR and considerations of the thermodynamic-radiative couplings presented in ESCAPE D3.3b. The specific aim of this work is to address whether the spread in the simulations of warming trends can be framed by these physical couplings. This would provide valuable guidance regarding the interpretation of the climatic projections provided by these models in spring prior to the monsoon.

Appendix A: Seasonal structure of the multi-decadal trend in surface thermodynamics

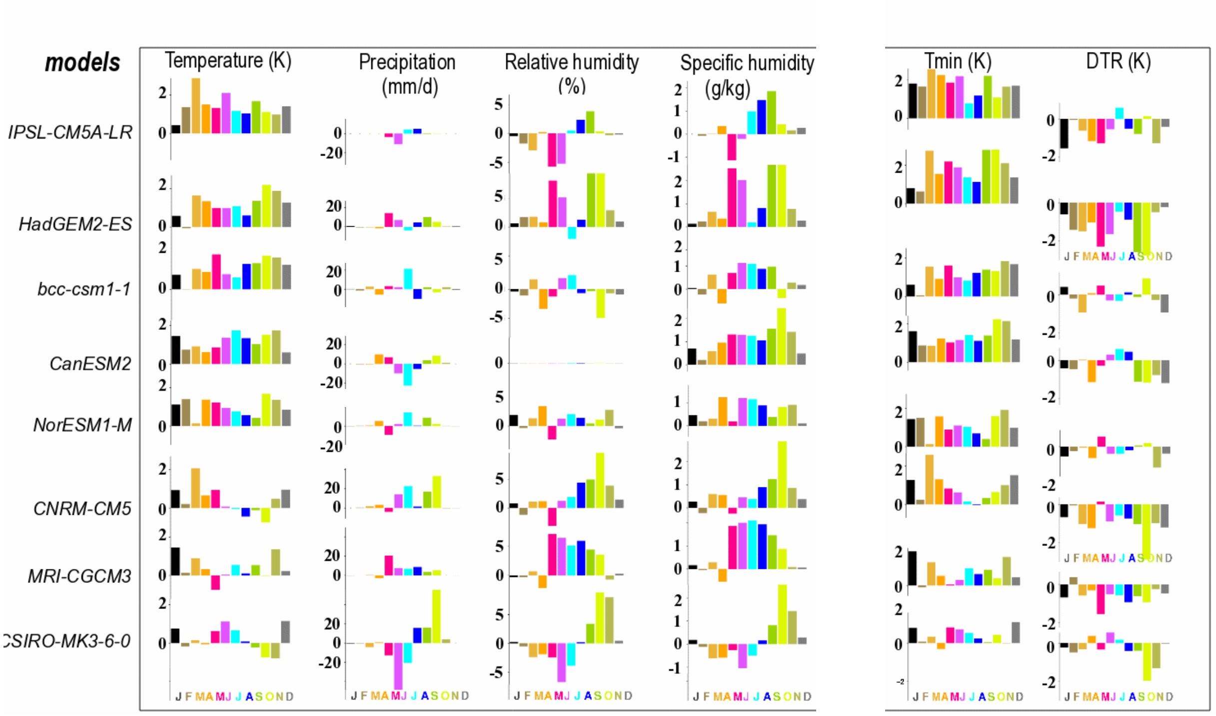

Figure A1*: Seasonal structure of the multi-decadal trend in surface thermodynamics and rainfall simulated between 1950 and 2010 with historical CMIP5 simulations at the closest point to Agoufou in central Sahel.*

REFERENCES

Christensen, J. H. and F. Boberg, 2012: Temperature dependent climate projection deficiencies in CMIP5 models. Geophysical Research Letters, 39 (24), L24 705.

Giannini, A., M. Biasutti, I. M. Held and A. H. Sobel, 2008: A global perspective on African climate. Climatic Change, 90, 359-383, doi:10.1007/s10584-008-9396-y

Guichard, F., L. Kergoat, E. Mougin and F. Hourdin, 2012:The annual cycle of temperature in the Sahel and its climatic sensitivity. AGU 2012. GC33A-1004.

Hourdin, F., I. Musat, F. Guichard, F. Favot, P. Marquet, A. Boone, J.-P. Lafore, J.-L. Redelsperger, P. Ruti, A. Dell' Aquila, T. Losada Doval, A. Khadre Traore and H. Gallee, 2009 : AMMA-Model Intercomparison Project, Bull. Amer. Meteor. Soc.. doi : 10.1175/2009BAMS2791.1

Hourdin, F., J.-Y. Grandpeix, C. Rio, S. Bony, A. Jam, F. Cheruy, N. Rochetin, L. Fairhead, A. Idelkadi, I. Musat, J.-L. Dufresne, A. Lahellec, M.-P. Lefebvre, and R. Roehrig, 2013a: LMDZ5B: the atmospheric component of the IPSL climate model with revisited parameterizations for clouds and convection, Clim. Dyn., 79, 2012. doi:10.1007/s00382-012-1343-y

Hourdin F., M-A Foujols, F. Codron, V. Guemas, J-L Dufresne, S. Bony, S. Denvil, L.Guez, F. Lott, J. Ghattas, P. Braconnot, O. Marti, Y. Meurdesoif, L. Bopp, 2013b: Impact of the LMDZ atmospheric grid configuration on the climate and sensitivity of the IPSL-CM5A coupled model, Clim. Dyn., doi: 10.1007/s00382-012-1411-3

Hulme M, 1992: Rainfall changes in Africa: 1931–60 to 1961–90. Int J Climatol 12:685–699

Hulme, M., R.M. Doherty, T. Ngara, M.G. New, and D. Lister. 2001: African climate change: 1900-2100, Climate Research, 17, 145-168.

Lamb, P. J., 1982: Persistence of Subsaharan drought. Nature, 299, 46-48. doi:10.1038/299046a0

Roehrig R., D. Bouniol, F. Guichard, F. Hourdin and J-L Redelsperger: The present and future of the West African monsoon: a process-oriented assessment of CMIP5 simulations along the AMMA transect. J. Climate, doi: 10.1175/JCLI-D-12-00505.1

Voldoire, A., et al., 2012: The CNRM-CM5.1 golbal climate model: description and basic evaluation. Clim. Dyn., doi: 10.1007/s00382-011-1259-y

D3.3b

Surface thermodynamics and energy budget couplings in West Africa: selected inferences from recent observations and their application to model evaluation

RESUME

Ce livrable présente une analyse physique des composantes radiatives du bilan énergétique à la surface et de ses couplages avec la thermodynamique et les précipitations en Afrique de l'Ouest. Les observations ont été utilisées pour identifier et caractériser les couplages dominants qui se manifestent au cours de l'année. Elles indiquent que le cycle annuel de rayonnement infrarouge à la surface est étroitement couplé au cycle de l'eau, à la fois dans l'atmosphère et à la surface. Les fluctuations du flux infrarouge net (*LWnet*) sont linéairement corrélées à celles de l'humidité relative à la surface (ou de manière équivalente au niveau de condensation) tout au long de l'année, des conditions les plus sèches aux plus humides. Le flux infra-rouge descendant (*LWin*) en revanche est aussi fortement modulé par d'autres facteurs que la vapeur d'eau dans les gammes de valeur d'eau précipitable inférieures à 30mm et on n'observe donc pas de relation linéaire entre les fluctuations de vapeur d'eau et de *LWin*. On montre ensuite que la différence des températures journalières maximales et minimales, *Tmax-Min*, encore notée *DTR*, est elle-même largement pilotée par le flux *LWnet*. Les observations indiquent cependant que d'autres processus limitent sensiblement l'amplitude de *Tmax-Tmin* en dehors des mois de mousson. Ces résultats sont étayés par des diagnostics quantitatifs élaborés à partir de données acquises au Sahel central et du nord pour la plupart, et couvrant plusieurs années.

Ces diagnostics ont ensuite été utilisés pour évaluer des modèles de climat participant à l'exercice CMIP5. Il s'avère que la plupart des modèles sont affectés par des biais importants (positifs ou négatifs) dans leur simulation du flux solaire incident et par une surestimation du flux radiatif net au printemps. Les causes de ces erreurs semblent impliquer de nombreux facteurs, allant de différences des propriétés et de l'état de la surface, jusqu'à l'ennuagement et la charge atmosphérique en aérosols (ces derniers modulant fortement le rayonnement solaire incident). Les diagnostics de couplage entre variables physiques permettent cependant d'analyser la validité des couplages simulés en se plaçant dans les gammes de valeurs effectivement reproduites par les modèles. On montre ainsi comment des couplages physiques qualitativement semblables mais distincts émergent dans les simulations climatiques. Cette analyse nous permet également de conclure que la surestimation de Tmax-Tmin observée dans de nombreux modèle hors de la période de mousson fait probablement intervenir un contrôle trop fort du rayonnement infra-rouge à la surface et non pas directement son amplitude.

1. Introduction

The importance of the surface energy budget (SEB) for the west African monsoon has been recognized for a long time (see Nicholson 2000 for a review of past pioneer studies), from both local and larger-scale considerations. The studies carried out within the AMMA project, which have been continued and extended within the ESCAPE ANR, now provide a renewed view of the interplay between the SEB and monsoon rainfall, but also, more generally, between the SEB and the annual cycle of surface thermodynamics, and about their coupled inter-annual variability.

The aim of this deliverable is to present selected findings inferred from exploration of these recent observations, with a particular focus on the annual cycle. After a short introduction to the annual cycle of surface net radiation, we will first discuss couplings emerging between surface longwave radiation (both surface upwelling and atmosphere downwelling fluxes) and the water cycle. The results underline that the impact of water on the SEB is really not restricted to surface wetting by monsoon rainfall. Second, motivated by the climatic fluctuations of the diurnal temperature range, *DTR* (e.g.; Karl *et al.* 1997), we have characterized this variable in more details with local data. Indeed, the amplitude of the *DTR* has decreased within a few decades over most land regions, and this decrease is particularly large over the Sahel (cf. D1.1.b). Specifically, we will show how surface net longwave radiation accounts for a large part of the large DTR fluctuations taking place within a year. Third, we will present results documenting the impact of rainfall on the SEB, from synoptic to interannual time scales.

Beyond improving our knowledge and understanding of the Sahelian climate, these results further provide physically-based diagnostics that we are currently using to evaluate climate models and this will be discussed and illustrated. In view of the more and more difficult questions for which climate model are solicited, it is of major importance to assess to which extend they are actually well suited, or not, to answer a range of climatic questions, either directly involving the SEB, or for which the SEB provides valuable information. This is relevant to issues such as the impact of climatic changes on the annual cycle of surface air temperature, or the timing and length of the pre-monsoon and monsoon seasons.

2. Surface net radiation

In the Sahel, the surface energy budget displays a very notable and non-intuitive annual cycle which is framed by both surface and atmospheric process as inferred from automatic weather station (AWS) data, across the AMMA-Catch sites (see Appendix A).

The left panel of Fig. 1 highlights important features of this cycle. First, the surface net radiation, R_{net} , almost equal to the sum of surface sensible and latent heat fluxes at daily-mean and larger time scales) is delayed with respect to the annual cycle of the incoming solar radiation at the top of the atmosphere (SW_{in}^{TOA}), and characterized by a sharp late summer maximum . This is not so usual, as the fingerprints of SW_{in}^{TOA} is often more pronounced on R_{net} , for example in the close Soudanian region (Fig. 1, right panel), where the cloud radiative impact is also higher. By contrast in the Sahel, monsoon rainfall happens to be a major driver of the sharp late summer rise of R_{net} , leading to substantial cooling of the soil (thus reducing the surface longwave emission) and allowing for vegetation growth (whose albedo is typically lower than the albedo of bare soil there). Therefore, this rise is typically less pronounced in the northern Sahel, where rainfall amounts become quite small (see purple curve in Fig. 1, left panel). Note however that it is comparable between the Agoufou Malian and Wankama Nigerien sites, and actually higher in Agoufou even though about 50% more rainfall was recorded at Wankama in 2006 (a result probably related to differences in vegetation cover, surface albedo and cloud cover). Overall, it appears that the core and late monsoon in the Sahel are characterized by a sharp rise of R_{net}, indicative of a strengthening of turbulent heat exchanges between the surface and the atmosphere.

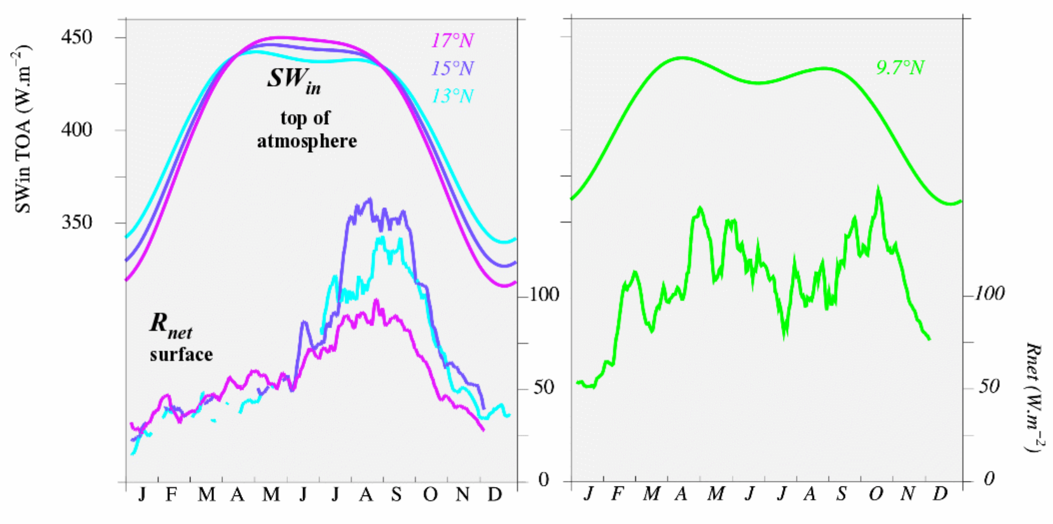

Figure 1 : Time series of top of the atmosphere incoming solar radiation (upper curve) and surface net radiation data (lower curve) for three Sahelian sites at different latitudes in the Sahel (left panel) and for a Soudanian site (right panel). The graphs are drawn for the year 2006 with AMMA-Catch data (Wankama 13°N, Agoufou 15°N, Bamba 17°N and Nalohou 9.7°N, and show 10-day running mean values.
(source of left panel : Guichard *et al.* 2012).
See appendix A for more information on the sites.

3. Couplings between surface longwave fluxes and the water cycle within the annual cycle

The annual dynamics of the water cycle in the Sahel is particularly strong. Both the atmosphere and soil turn from very dry in winter to very moist[1], cloudy and wet during the monsoon. This contributes as much as the annual cycle of the insolation to shape the surface radiation, water and energy balances, as illustrated below with selected results.

Hereafter, we consider complementary variables to characterize atmospheric water vapour. First, regarding the humidity of air at the surface, we make use of the lifting condensation level rather than air relative humidity measured by the AWS 2m above the surface (RH_{2m}). In short, the lifting condensation level corresponds to the pressure at which an air parcel becomes saturated, when adiabatically lifted from the lower atmosphere (here from 2m). Thus, the lifting condensation level, which closely mirrors RH_{2m} in units of pressure height, is also a valuable proxy for cloud-base height (Betts 1997). Note that it is expressed here as a departure from surface pressure Ps, and noted (P_s-P_{lcl}) so that low (P_s-P_{lcl}) values correspond to high RH_{2m} values and vice-versa.

3.a) Surface net longwave flux and humidity

First, we focus on the net surface longwave radiation, LW_{net}, the difference between the surface incoming and upwelling longwave flux. It can be thought of as a measure of the thermal (de)

1 *In term of water vapour amount, as measured for instance by precipitable water, which can be very high in summer, even though the relative humidity remains moderate during daytime as a result of elevated temperatures.*

coupling between the surface and the atmosphere[2], with a stronger decoupling indicated by more negative values of LW_{net}, when the surface emission is much higher than the emission of the atmosphere directed to the surface.

This is the case when the atmosphere is drier (i.e. at lower RH_{2m} here, or equivalently at higher P_s-P_{lcl}). The drier situations typically correspond to late winter, early spring days, when the dry land surface is very hot and the opacity of the atmospheric column, also dry, still low. On the other hand, during the monsoon, the wetter cooler surface emits less, and the moist and cloudy atmosphere, even if somewhat cooler, still radiates more towards the surface. Such radical differences in soil and atmosphere water amounts are expected to lead to large fluctuations in the magnitude of LW_{net} throughout the year.

Figure 2 : Scatter diagrams of lifting condensation level versus surface net longwave flux.

The graphs are made with daily-mean values, and use multi-year data of the automatic weather station of the Agoufou site in Mali (Mougin et al. 2009), colours identify months.

Note that very similar relationships emerge with data from the other AMMA Catch Sahelian sites of Mali and Niger, and from the ARM mobile facility installed in Niamey in 2006 as well. These are also reasonably well reproduces by the ECMWF analysis (see Appendix B).

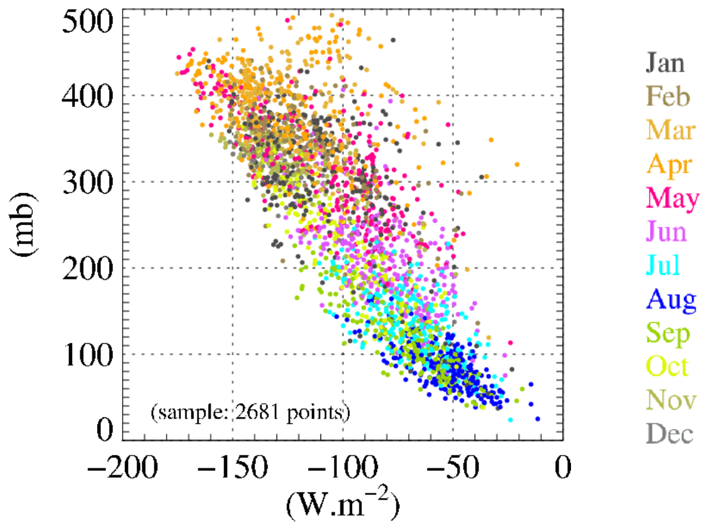

Figure 2a indeed underlines the strong magnitude of humidity (P_s-P_{lcl}) and LW_{net} fluctuations, but it also shows an obvious coupling between them[3]. The figure further implies that the mechanisms discussed above may control these coupled annual fluctuations, beyond the scatter driven by other processes operating at the smaller time scales. Among them, the radiative impact of mineral aerosols, whose optical depth is higher outside of the core monsoon, could play an important role. This would be consistent with the larger scatter characterizing drier days (P_s-P_{lcl} higher than 140 mb). This could also involve mid-level stratus clouds which are frequently occupying the top of the Saharan air layer, during the monsoon months (Stein *et al.* 2011), but also in spring, when their radiative impact in the longwave is typically more pronounced, within a drier atmosphere (Bouniol *et al.* 2012, see also Stephens *et al.* 2012). Couplings between LW_{net} and RH_{2m} were identified by Guichard *et al.* (2009) for the Sahel. However, they only considered the months of June to September, when daily-mean (P_s-P_{lcl}) essentially remains below 250 mb (or, equivalently, daily-mean RH_{2m} remains above 30%). Fig. 2a indicates that this coupling holds over a much broader range. Note that Betts (2004) also emphasized such a coupling, but in less arid climatic zones, for (P_s-P_{lcl}) always lower than 140 mb. Our results, which document very dry conditions, suggest a possible influence of clouds even in fairly arid atmospheric conditions, when

2 *Note that this thermal coupling involves interactions between longwave radiation and the other components of the SEB, they are typically stronger during daytime and weaker during nighttime when turbulent and ground heat fluxes are both weaker.*

3 *Note that the scatter diagram (Fig. 3a) would be very similar with RH_{2m} instead of (P_s-P_{lcl}), with fluctuations of RH_{2m}, $\delta RH_{2m} \sim - \alpha\, \delta (P_s\text{-}P_{lcl})$ [$\alpha > 0$]*

clouds typically cannot form in the few first kilometres of the atmosphere because thet are too dry and cloud base heights typically remains 3-4 km above the ground.

3.b) *Surface incoming longwave flux (LW_{in}) and atmospheric water vapour amount*

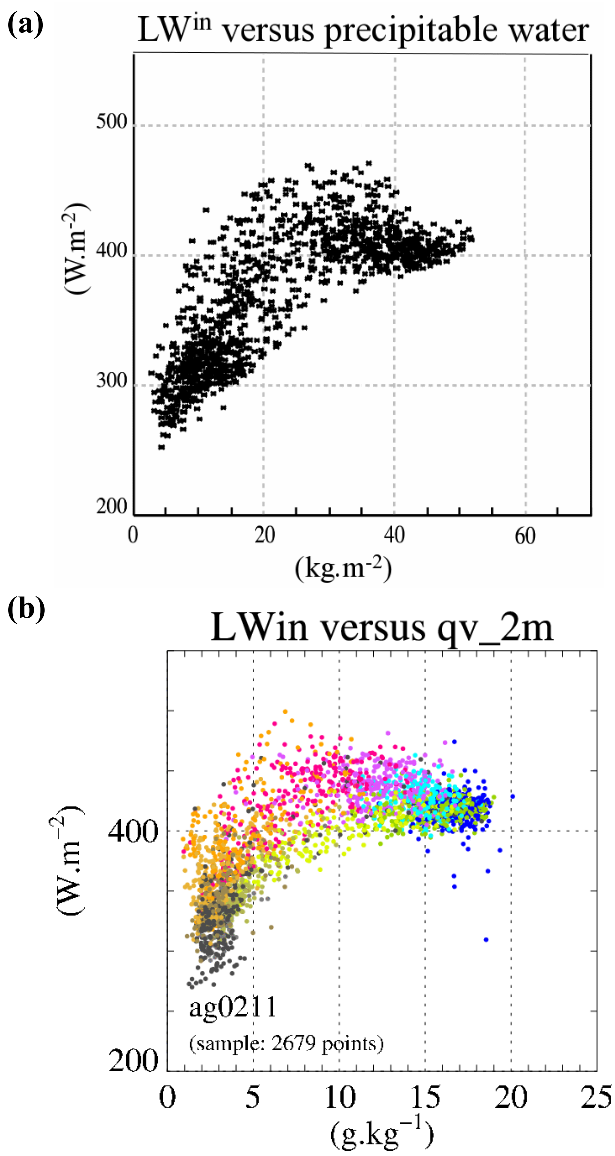

Figure 3 *: Scatter diagrams of surface incoming longwave radiative flux versus precipitable water (a) and specific humidity at 2m, qv2m (b).*

The graphs are made with daily-mean values, and use data of the automatic weather station of the Agoufou site in Mali, plus, in 3b GPS estimates of precipitable water from Gao (Bock et al. 2008). Note that both datasets are available over several years, with a common window extending over more than three years.

Note that very similar relationships emerge with data from the other AMMA Catch Sahelian sites of Mali and Niger, and from the ARM mobile facility installed in Niamey in 2006 as well (see Appendix C).

The structure and scatter are about the same with the better co-location of GPS and automatic weather stations in Niger, likely because the overall coupling found here is largely determined by large-scale changes arising within the annual cycle, furthermore daily-mean values are expected to be associated with - representative of - larger spatial scales than instantaneous values.

As previously discussed, the surface incoming longwave radiative flux is expected to be affected by atmospheric water, and this has long been taken into account in numerous empirical formulations (e.g. Prata 1996, Dilley and O'Brien 1998). This sensitivity was studied in more details at Niamey with the ARM data available in 2006 (Slingo *et al.* 2009). The latter showed the expected broad increase of LW_{in} at higher values of precipitable water (*PW*, the total amount of water vapour within an atmospheric column) but also underlined compensating effects between atmospheric temperature (cooler versus warmer) and water vapour amount (more versus less). The results presented in Fig 3b are indeed very consistent with Slingo *et al.* (2009). Furthermore, because of the larger size of the sample provided by the AMMA EOP dataset, they show more clearly that LW_{in} is not the highest during the monsoon, when *PW* reached its annual maxima, but for intermediate *PW* values, corresponding to spring days, when the atmospheric column is very warm, already sometimes cloudy, even if less, and often heavily loaded in aerosols. Fig. 3b also indicates a maximum of fluctuations during this period, and this can be interpreted as the '*PW* window' within which aerosols and clouds are able to influence more substantially the surface incoming longwave radiation LW_{in} than later, during the monsoon.

4. Couplings between surface longwave fluxes and surface air temperatures

It is well known that surface air temperature quickly responds to insolation within a day, with the higher temperatures typically reached in summer on clear sunny days (in the midlatitudes). However, the annual cycle of daytime mean temperature T_{2m} is more directly connected to surface skin temperature T_s , or LST for land surface temperature in the Sahel (e.g. see Figs. 1 and 11a of Guichard *et al.* 2009). Jin and Dickinson (2010) emphasize the distinct physics underlying both variables. Our analysis of local observations, based on T_{2m} , and surface upwelling flux in the longwave from which we define a proxy for T_s , is indeed well in line with their findings. The diurnal cycles of T_s and T_{2m} are distinct, as well as the seasonal fluctuations of these cycles; the daily-mean difference T_s - T_{2m} is also found to steadily increase with T_s from typically less than 1°C below 30° to about 4°C at 40°C for the Agoufou site (not shown). Still, from an annual cycle perspective, fluctuations of T_{2m} appear to be very tightly framed by T_s at local scale in the Sahel (not shown). This coupling is probably strengthened by the specificities of the Sahelian climate. In particular, soil moisture constrains evapotranspiration and cloudiness is relatively low in this region, and both of these factors favour the direct influence of the land surface on surface air temperature.

By contrast, the fluctuations of minimum and maximum temperatures are less strongly coupled to daily-mean values of T_s and T_{2m}, and the annual cycle of their difference, the diurnal temperature range, $DTR = T_{max}$-T_{min}, is poorly related to T_s. Interestingly, Betts (2006) proposed a scaling of *DTR* by the daily-mean surface net longwave radiation. More precisely, he introduced a radiative *DTR*, DTR_{RAD} , via a simple formulation of the fluctuations of *T* due to longwave radiation, defined as:

$$DTR_{RAD} = (-4\sigma T^3) / LW_{net}$$

where $\sigma = 5.67\ 10^{-8}$ W m^{-2} K^{-4} is the Stefan-Boltzmann constant.
His study focussed on the warm season nocturnal boundary layer in different regions of northern and southern America during the warm season, and made use of meteorological reanalyses data to test the relevance of such a scaling. Hereafter, we show that his proposal is indeed quite useful to explore observations of the annual cycle of *DTR* within the distinctive Sahelian climate as well.

The upper panel of Fig. 4 shows from left to right the monthly-mean diurnal cycles of surface air temperature (T_{2m}), T_{2m} departure from daily-mean, and normalized T_{2m} departure from daily-mean (see legend for more details) in the northern Sahel (Bamba site). The same fields are presented for the Agoufou site in the lower panel.The magnitude of the fluctuations of *DTR* and daily-mean temperatures from month to month are in the same range. Not surprisingly, *DTR* is the larger during the drier spring months, with strong nighttime cooling and daytime warming. More surprising, and valuable, is the strength of the tested normalization (left panels). It is particular obvious in Bamba, where the monthly-mean diurnal curves are almost identical[4]. In other words, a knowledge of the monthly-mean values of LW_{net} and temperature is enough to recover most of the monthly mean *DTR*. In practice the sensitivity to temperature is much weaker and the use of yearly-mean instead of monthly-mean temperatures yields very close results.

4 *In Agoufou, the scatter appears to be partly related to the imprint of several disturbed cloudy and rainy days in August and September.*

(a)

(b)

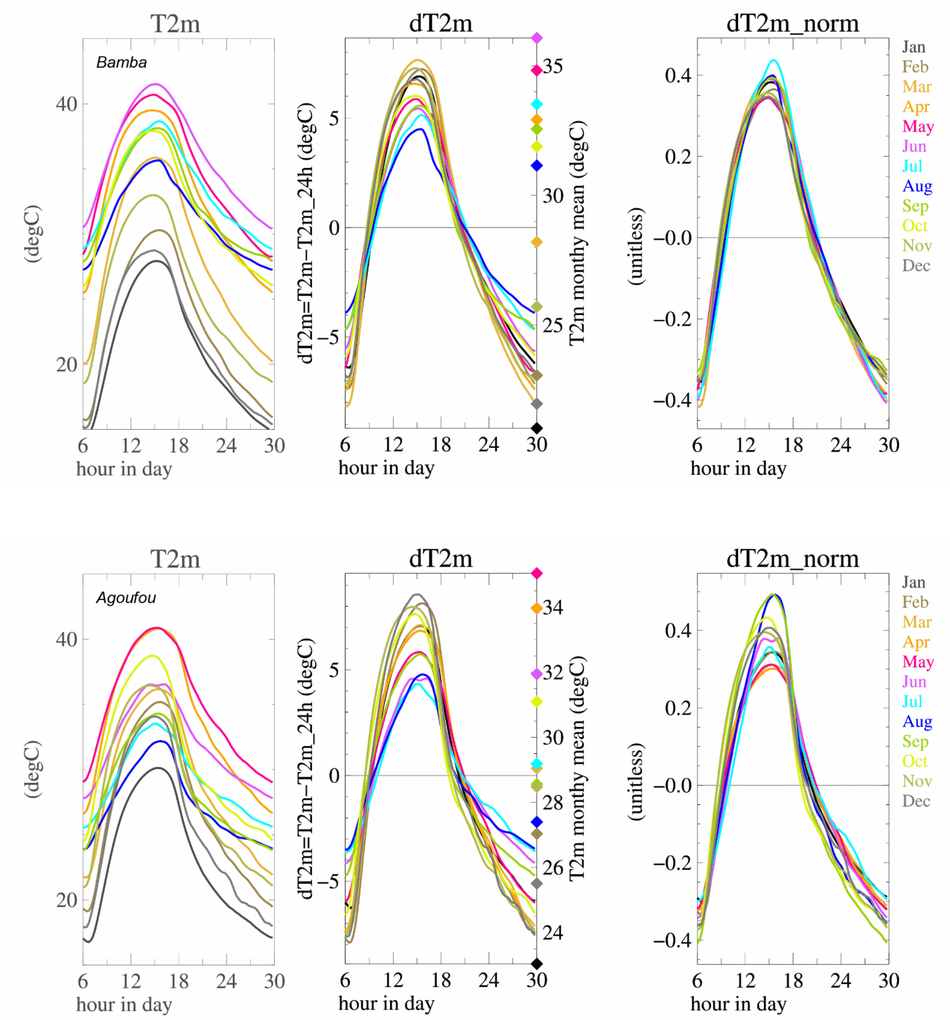

Figure 4 *: Monthly-mean diurnal cycles of surface air temperature variables in (a) Bamba and (b) Agoufou for: left panels T_{2m} (hereafter T) middle panels $\delta T = T - \overline{T}$ and right panels $\delta T_{NORM} = (-4\sigma \overline{T}^3).\ \delta T\ /\ \overline{LW}_{net}$*

T, δT, δT_{NORM} : F (hour, month) ; for any variable α, $\overline{\alpha}$: F(month) corresponds to the monthly mean of α.
Colours identify months and, in middle panels, diamonds on the right y-axis indicate values of $\overline{T}$.
In middle and right panels, the left y-axis are scaled by the minimum and maximum of respectively δT and δT_{NORM} so that the scatters among months in the two figures can be graphically compared.
The time axis is from 6h to 6h the next day so as not to cut the nighttime period, and data from 2006 (2003) have been used for the Bamba (Agoufou) plots.

This is further illustrated with scatter plots of DTR versus DTR_{RAD} (Fig. 5). During the core of the monsoon, in August, DTR_{RAD} is very close to DTR[5], but smaller during the other months (see also Appendix D). The slope is about 0.5-0.6, not one, for the monthly-mean values and the maximum DTR is about 15 instead of 20 given by DTR_{RAD} (Fig. 5, right). These results are consistent with Betts (2006) although the causes for the slopes lower than 1 possibly differ. He identified the short nighttime duration in summer at midlatitude sites where the slopes were also less than 1 as an important factor. Here, a more obvious potential candidate is advection, notably during the establishment of the monsoon when it is the stronger. Nighttime turbulent processes may also play a

5 *It is even higher in Agoufou, due again to the numerous perturbed cloudy and rainy days, and they will be discarded in a second step.*

more important role in observations than in the ECMWF reanalyses considered in Betts (2006). Especially the ECMWF model, as several other models, is characterized by its tendency to vertically mix the stable boundary layers too much via parametrized turbulent processes (Sandu *et al.* 2013), and such a functioning tends to weaken the sensitivity of turbulence to the stability of nocturnal boundary layers. The same limitation may apply to the recent study of Jackson and Forster (2010) as their radiative estimate were provided from ECMWF reanalyses as well. (see Appendix D for more details.)

Figure 4 (right panels) also indicates more subtle changes in the structure of the diurnal cycles, with a more gradual morning heating in August and following months compared to earlier months. Such patterns cannot be addressed with this scaling. On the other hand, they can be understood from knowledge on the vertical structures in the lower atmosphere, surface and boundary layer convective dynamics and clouds, at least at first order (Gounou *et al.* 2012). For instance, during the core of the monsoon, surface sensible heat fluxes are typically smaller and the lower atmosphere more stable, so that both contribute to slow down the daytime heating.

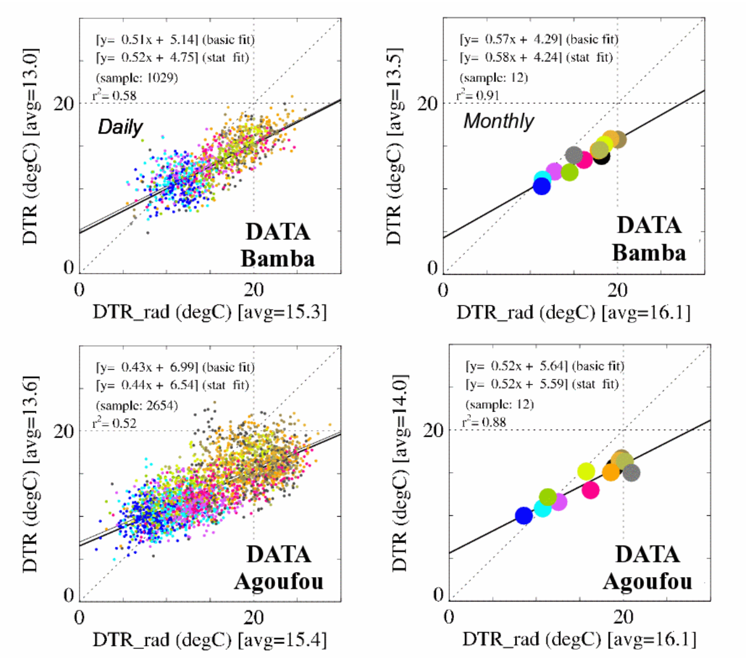

***Figure 5** : Scatter plots of daily (left) and monthly (right) mean DTR versus DTR $_{RAD}$ in Bamba (top) and Agoufou (bottom).*

The colour code identifies months (same conventions as in Fig. 2).

5. Couplings between monsoon rain and SEB: from synoptic to interannual scales

In sections 3 and 4, we identified and documented how some physical couplings between surface radiation, atmospheric water and temperature operate in the Sahel and shape the observed annual cycle. During the monsoon, surface processes are also directly affected by precipitation and this is generally better recognized, intuitively and qualitatively. A more quantitative knowledge is currently being drawn from data as illustrated below.

Recent works include Lohou *et al.* (2013), who document the observed modifications of the surface evaporative fraction *EF* (i.e. the ratio of surface latent heat flux to the sum of surface sensible and latent heat fluxes) that are driven by precipitation at synoptic scale. The results, consistent with basic physical understanding, demonstrate a particularly strong and short-lived surface response for the Sahelian sites (Fig. 6), contrasting with the much weaker influence of rainfall for more southern locations at this time scale (Lohou *et al.* 2013). The study also identifies a damping impact of vegetation on EF fluctuations, which is coherent with the capability of vegetation to extract water from deeper soil layers when bare surfaces are dry and do not evaporate (compare green curve with orange curve for bare soil). Thus, EF, and more widely the SEB, is characterized by substantial fluctuations from day to day in the Sahel, especially prior to vegetation growth or over bare soil, and these fluctuations provide critical contributions to the SEB. An evaluation of the land surface models (LSM) which participated to the ALMIP model intercomparison exercise (Boone *et al.* 2009) further reveals a qualitative agreement but substantial scatter too in the response of EF to rainfall among LSM. As the same LSM are used in land surface-atmosphere coupled climate models, this result casts doubts on the ability of these models to all reproduce this basic functioning with enough accuracy, beyond other errors introduced by specific features of the simulated rainfall field, i.e. too frequent and weak rainfall events, shifted too early in the diurnal cycle. Therefore, it appears reasonable to expect that the impact of rainfall on the SEB in climate simulations departs from observations in various ways, and this is likely to further influence the type and scale of the couplings that can actually operate in models.

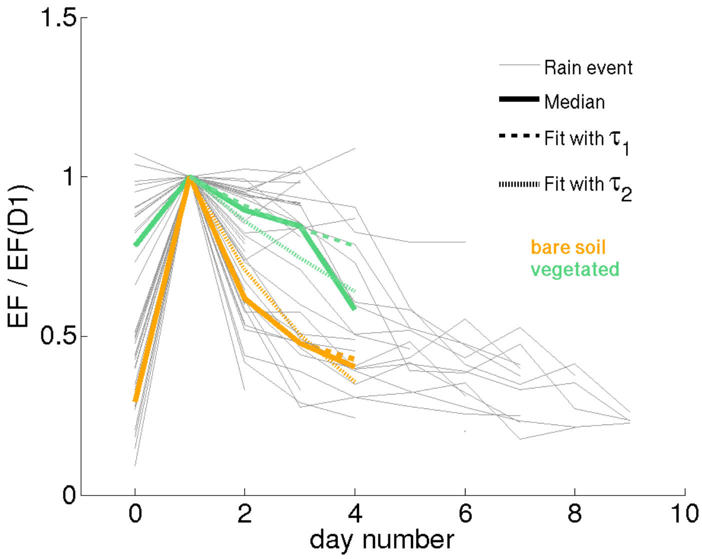

Figure 6 *: Links between rainfall and the surface energy balance at synoptic scales. Evolution of the daily normalized evaporative fraction (EF, the ratio of the surface latent heat flux to the sum of surface sensible and latent heat flux) before and after rain event for the grass land site of Agoufou (Mali). Thin grey lines stand for individual rain events, the orange (green) curve corresponds to the median of rain events over bare (vegetated) soil. Dotted and dashed lines stand for two distinct exponential fits. Here, EF is normalized by its value on the day following a rainfall event - see Lohou et al. 2013 for more details.*
(Source: adapted from Lohou *et al.* 2013)

At larger time scales, we identified another coupling, which emerges between the inter-annual fluctuation of JJAS rainfall and surface longwave emission. Namely, a more rainy summer locally couples with a cooler surface which emits less radiation (Fig. 7). This result is qualitatively intuitive, but its quantitative interpretation is not trivial, neither the smooth curve that can be drawn by eye from individual dots in Fig. 7 (see also appendix E). Indeed, more rain is expected to be associated with more surface evaporation, and therefore less daytime warming of bare soil. However, this is not clue as to why an average 1 mm.day-1 increase in rainfall (roughly equivalent to 30W.m-2) couples with a drop of about 10W.m-2 in LWup. A comprehensive explanation of this result may requires further analysis of surface and soil properties, energy and water budgets, with considerations of the influence of vegetation growth and associated transpiration together with changes in surface albedo (Samain et al. 2008), as well as consideration of cloud radiative forcing at the surface, especially in the shortwave. Furthermore, the results of Lohou et al. (2013) show the interest to explore further how this difference is realized down to daily time scales.

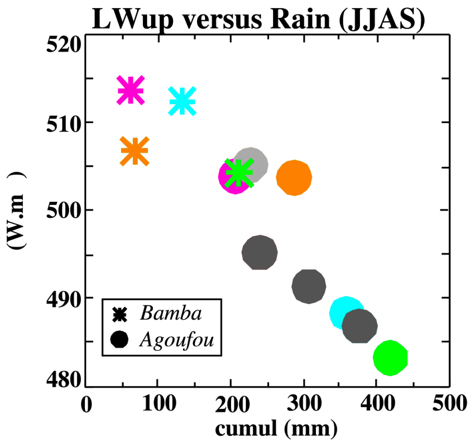

Figure7 *: Links between rainfall and the surface energy balance at longer time scales.*
(b) *JJAS average surface upwelling longwave radiation (LWup) versus precipitation in Agoufou and Bamba for different years. The coloured dots stand for different years.*
It is important to note here that LWup rather than LW_{in} (which is about the same from one year to the other here) accounts for a large part of the inter-annual fluctuations of R_{net} during the monsoon (see also Appendix E).

6. Evaluating models

The results presented in previous sections call for in-depth studies in order to clarify and to quantify better the contributions of each potentially influential factor in the relationships identified between surface thermodynamic and SEB. Still, they already provide evidence of major couplings arising between the water and energy cycles at the surface in the Sahel together with synthetic diagnostics to characterize them, either during the monsoon (section 5) or throughout the year (sections 2, 3, 4).

From a modelling perspective, and related to the issue of climate projections, it is important to address the extend to which climate simulations are able to reproduce these couplings and, further, to assess the influence of different controlling factors (e.g. for LW_{in} this involves atmospheric temperature, water vapour, clouds, aerosols). For a given simulation, a lack of clouds, a neglect of dust aerosol radiative effects, or conversely an overly strong aerosol or cloud radiative impact, all may lead to misshaped couplings, with different structures or mean slopes. On the other hand, regardless of any mean slopes, a too long (too short) simulated monsoon season would probably lead to different scatter diagrams, with more occurrences in the moister (drier) sectors of the diagrams. Such physically-based analyses help interpreting, and further, they provide guidances for improving climate simulations.

Following the work initiated by Hourdin et al. (2010) on the evaluation of climate models over west Africa, we are currently working on this issue using CMIP5 climate model dedicated outputs as explained in ESCAPE D3.3a. This includes in particular thermodynamic and energetic diagnostics at selected locations along the West African meridional climatological transect. For this evaluation of the mean climate, we are using amip type 30-year long simulations for reasons explained in Roehrig *et al.* (2013). However, our conclusions remain unchanged when considering historical type simulations for instance, because the spread among models largely dominates over the differences among distinct types of simulations performed with a single model. Note also that the main differences among models persist when considering the different sampled locations along the transect (see examples in Appendixes).

The structure of the annual cycle of the SEB is not discussed below but the comparison to observations emphasizes a too approximate and smoothly varying annual cycle in models, and a very large overestimation of surface net radiation in spring, as already pointed out by Traore (2011) for CMIP3-type models (see Appendix F). It is worth mentioning here that a comparison of simulated and observed R_{net} does not necessarily appear the most informative, because it integrates various sources of differences, related to surface properties and state (e.g. differences in albedo, soil moisture...) and to the atmospheric state (temperature and water vapour, but also clouds and aerosols). As a matter of fact, the differences in R_{net} , even if not negligible, are surprisingly smaller than in surface incoming shortwave radiation in the Sahel, the latter reaching more than 50 of $W.m^{-2}$ in monthly mean values. It appears that this unexpected finding is well explained by consideration of a chain of compensating differences in the components of the surface radiative budget (not shown). It is also notable that the differences in clear sky SW_{in} are still very large (a few tens of $W.m^{-2}$), and probably involve a radically different treatment of aerosols (see Appendix F).

Figure 8 illustrates of the differences in the observed and simulated couplings discussed in sections 3 and 4. In short, couplings arise in all models and they are broadly similar to observed couplings and physically sound, but they are quantitatively different. In addition, we suspect errors in some CMIP5 files for two models, namely CanAM4 (in cyan) and EC-Earth (in pink) (see results for other sites in Appendix I).

Among the various inferences that can be drawn from Fig. 8, it is notable that the MIP-ESM-LR model departs from the other models in terms of coupling between longwave radiation and atmospheric water vapour, with much higher LW_{net} for a given relative humidity (or P_s-P_{lcl}). This involves differences in LW_{in} on the order of tens of W.m-2 at comparable values of q2m and precipitable water. The overall larger values of LW_{net} (and thus smaller DTR_{RAD}) in this model at least partly account for its too small *DTR*. On the other hand, the other models (discarding Canam4 and EC-Earth here) display a somewhat too wide range of DTR_{RAD} values, but it is mostly ther too steep slope (close to 1:1) which explains the overestimate of *DTR* in these models. These first analyses need to be refined but they already point to the interest of a joint evaluation of surface longwave radiation and temperature in future investigations of *DTR* and *DTR* climatic fluctuations.

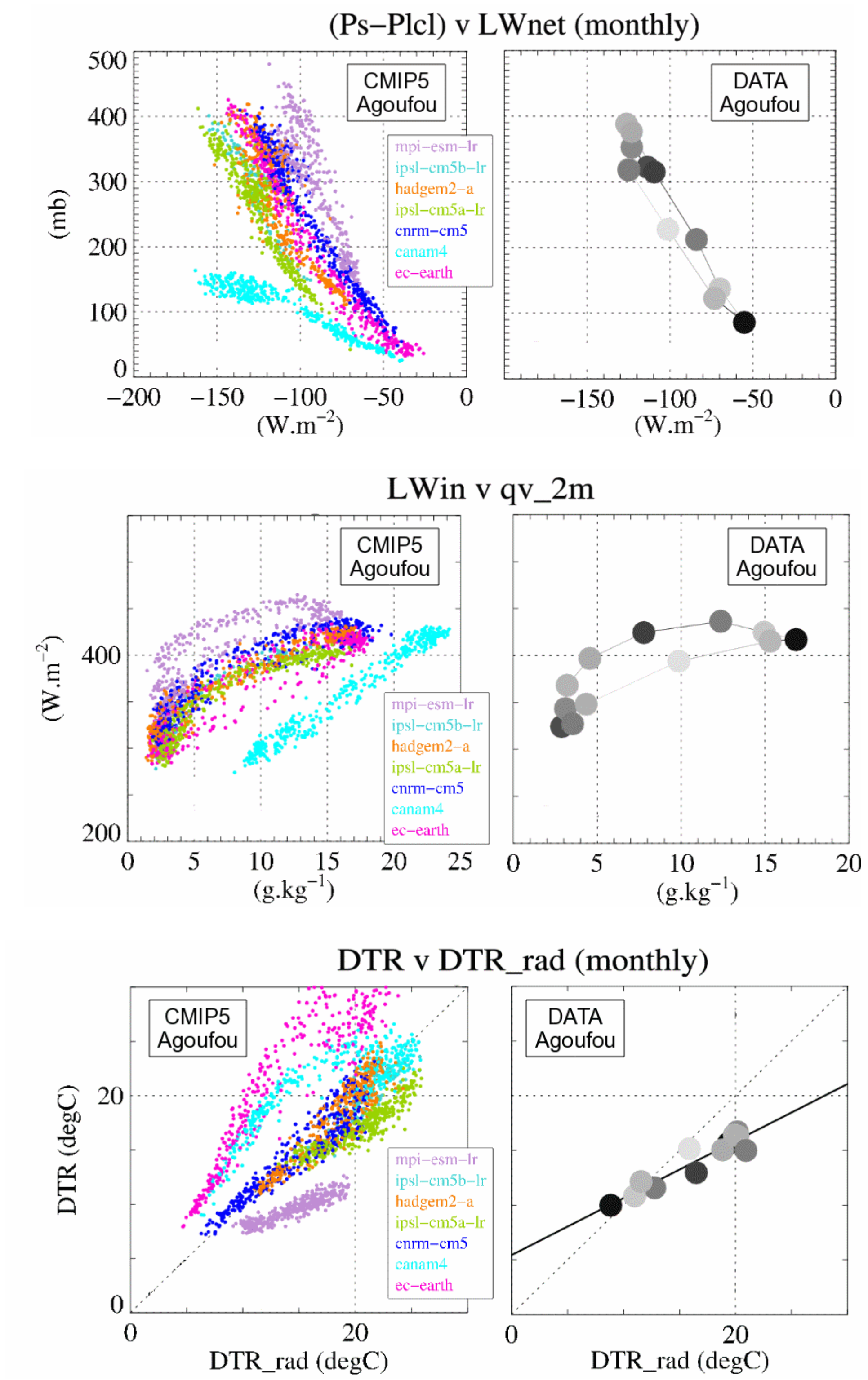

Figure 8 *: Scatter diagrams of monthly-mean P_s-P_{lcl} versus LW_{net} (top), LW_{in} versus qv2m (middle) and DTR versus DTR_{RAD} (bottom) in models (left panels) and observations (right panels) for the Sahelian site of Agoufou.*
(see Appendix G and H for more details at other sites and finer time scales.)

Focussing now on the monsoon period, in section 5 we identified strong connections between rainfall and LWup during the monsoon. As shown in Fig. 9, when focussing on a given Sahelian location during the monsoon, part of the model spread is associated with differences in simulated rainfall This is also why data from Bamba are considered here as well, as they provides a more relevant reference for the drier (in terms of rain) models (IPSL-CM5a-LR, IPSL-CM5b-LR and HadGEM2-a). A few models actually display coupled inter-annual fluctuations of rainfall and LW_{up} which appear similar to observations (notably CNRM-CM5). However, it is not possible to draw valuable conclusions when the range of simulated rainfall is too far from observed and it would be necessary to add observations from the Niger site in order to evaluate the wetter model (namely CNRM-CM5, CanAM4 and EC-Earth). The results are also interesting for the interpretation of model spread. Indeed, apart from EC-Earth and MIP-ESM-LR, the spread in simulated LWup and rainfall appear to be linked.

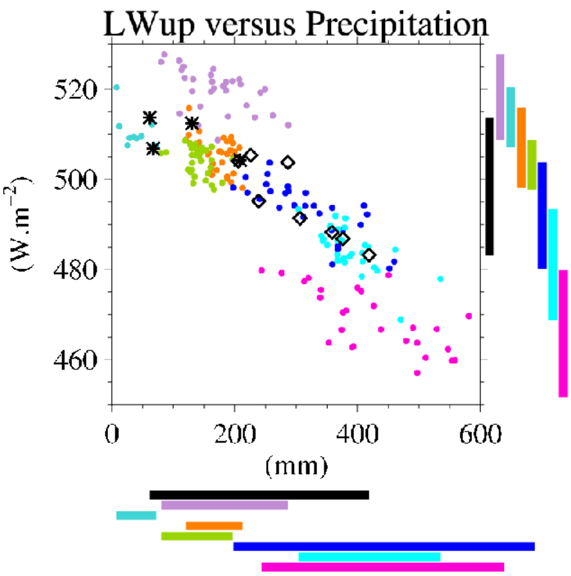

***Figure 9**: Scatter diagram of Lwup versus rainfall (JJAS), climate models (colours dots) and observations (black symbols, diamonds for Agoufou and crosses for Bamba). The horizontal and vertical segments on the bottom and right sides extend from the minimum and maximum values reached by each model and observations.*

From observations, we identified LWup as a major driver of the interannual variability of R_{net} during the monsoon (cf Appendix E), the more precipitating monsoon being typically associated with the higher values of R_{net} (Fig. 10, top panel). In contrast, the inter-annual variability of R_{net} in models remains lower, even for the models which simulate substantial inter-annual variability of rainfall. In fact, each model occupies a given range of R_{net} values without much fluctuations from one year to the other. In addition, the more rainy models are also characterized by a lower R_{net} (CNRM-CM5 and EC-Earth), as opposed to observations. CanAM4 stands as an outlier and this appears to involves its surface albedo, about 0.1 less than in the other models. A closer inspection of the surface radiative budget further indicates that SW_{in} is a major driver of these differences among models, and for several of them, SW_{in} is lying outside of the range of values provided by observations (Fig. 10, lower panel).

Overall, these first evaluations of the SEB and thermodynamic-energetic couplings highlight that important issues remain in terms of climate modelling over the Sahel, and these issues are not limited to the simulation of the monsoon season, indeed, the spread in *DTR* and radiation increases when moving to drier conditions (e.g. Fig. 8 bottom). Furthermore, the differences among models persist from the soudanian to the Sahara; this suggest that many underlying causes are to be found in their distinct formulation of the parametrized physics.

Figure 10 *: Scatter diagram of R_{net} versus rainfall (lower panel) in models and observations (top panel) and comparison of the surface radiative fluxes SW_{in} , SW_{up} , LW_{in} , LW_{up}, R_{net} and precipitation (lower panel).*
The colour and symbol codes are the same as in previous figure. For models, each horizontal segment corresponds to a different year.
The values correspond to a 2-month average, spanning mid-July to mid-September.

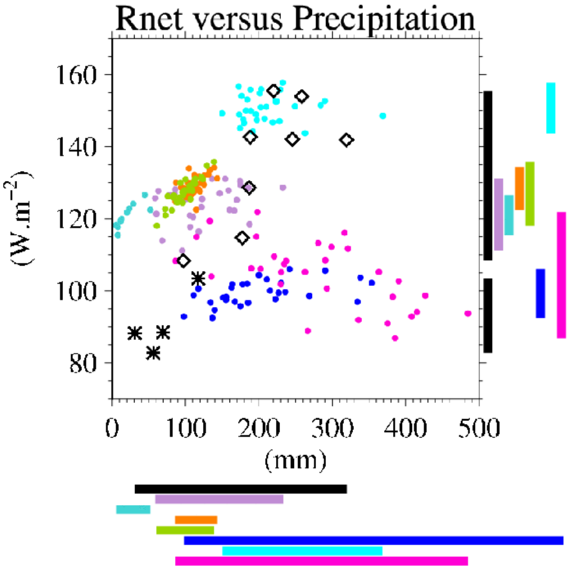

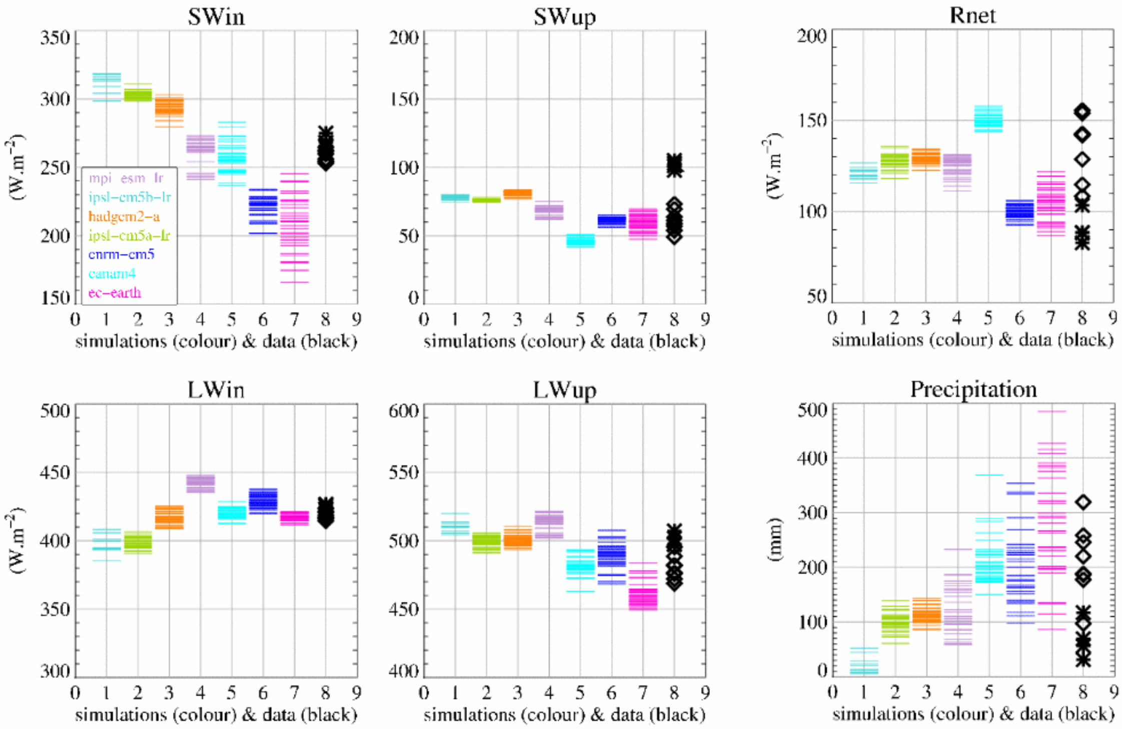

Conclusion

This deliverable presented our recent work on the surface energy budgets and its couplings with thermodynamics in the Sahel. Our results show that the annual cycle of surface longwave radiation is closely linked to the water cycle, both in the atmosphere and at the surface. The surface net longwave radiation in turn appears as a major driver of the diurnal temperature range, a very important and climate sensitive variable. These findings are supported by quantitative diagnostics elaborated from observational datasets acquired, for most of them, in the central and northern Sahel and covering a few to several years. The data from the AMMA database have been used here, and in order to extend these results in the future, it would be valuable to incorporate additional datasets from the Niger and Soudanian sites. As briefly mentioned, connections between *DTR* and LW_{net}

have been studied for the most part with the help of meteorological reanalyses, and local data such as used here are valuable and useful because they provide a more reliable characterization of surface radiation.

These diagnostics can be further used to evaluate CMIP5 climate models, and we provided some examples. Results already point to very large inaccuracies in the SEB, in particular in the surface incoming solar radiation (monthly mean biases reach several tens of $W.m^{-2}$). Because these biases are partly compensated by other errors, differences in surface net radiation, even if non negligible, are not as spectacular. However, this functioning raises issues regarding sensitivity studies performed with such biased simulations, as they can be dominated by mechanisms which are not operating in reality. The bias in SW_{in} in particular appears to involve radiative impacts of clouds, but also of aerosols in clear sky conditions, and the latter were found to substantially differ from one model to the other. Finally, as mentioned by other studies (e.g. Kothe and Ahrens 2010), we noticed that the surface albedo of many models does not appear accurate enough. In a next step, the coupling that we have identified should be helpful to interpret model spread, and possibly, model climatic sensitivity. In particular, extending the coupled (DTR, LW_{net}) observational analysis and model inter-comparison illustrated above would further our understanding of the mechanisms at play in reality and in climate simulations.

Appendix A: location and precipitation climatology of the AMMA-Catch sites

(a)

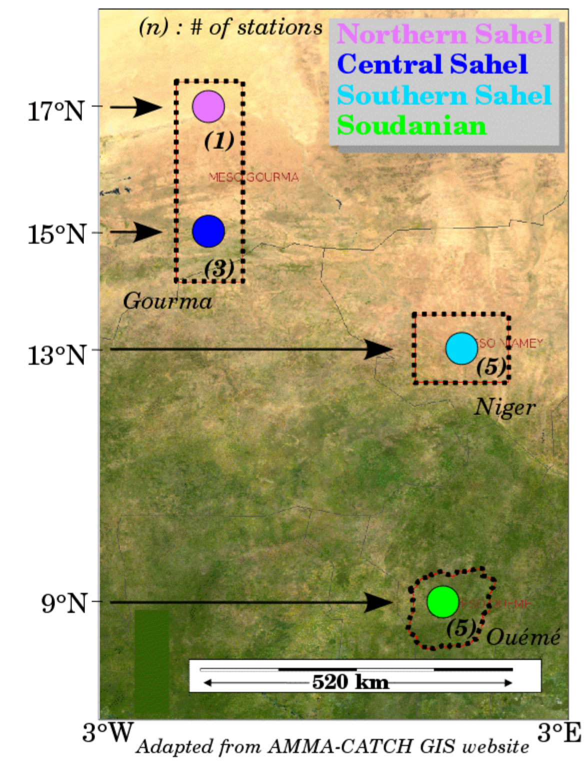

(b)

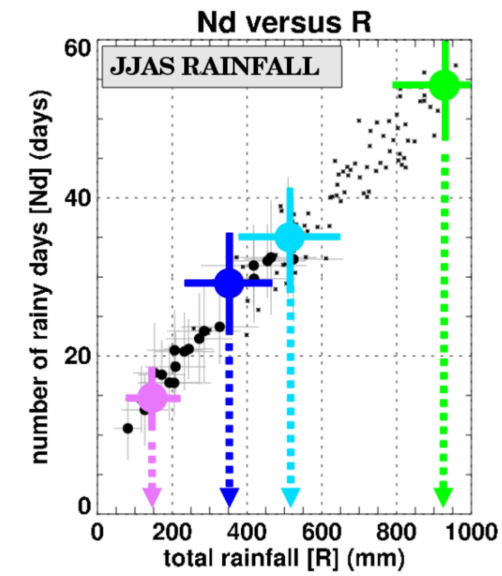

***Figure A1**: location of the different sites used to prepare Fig. 1(left panel) and JJAS rainfall climatology for these different sites (right panel) - same colour code as in Fig. 1.*
The JJAS rainfall was computed from multi-decadal data provided by historical SYNOP for the Benin and Niger sites using data of the nearby Djougou and Niamey stations resp., and for the Malian sites the data of Hombori and Bamba stations presented in Frappart et al. (2009). Nalohou lies within the Ouémé basin, and Wankama is part of the mesoscale Niger site.

Appendix B : Coupling between (P_s-P_{lcl}) and LW_{net} at different sites in observations and in the ECMWF model

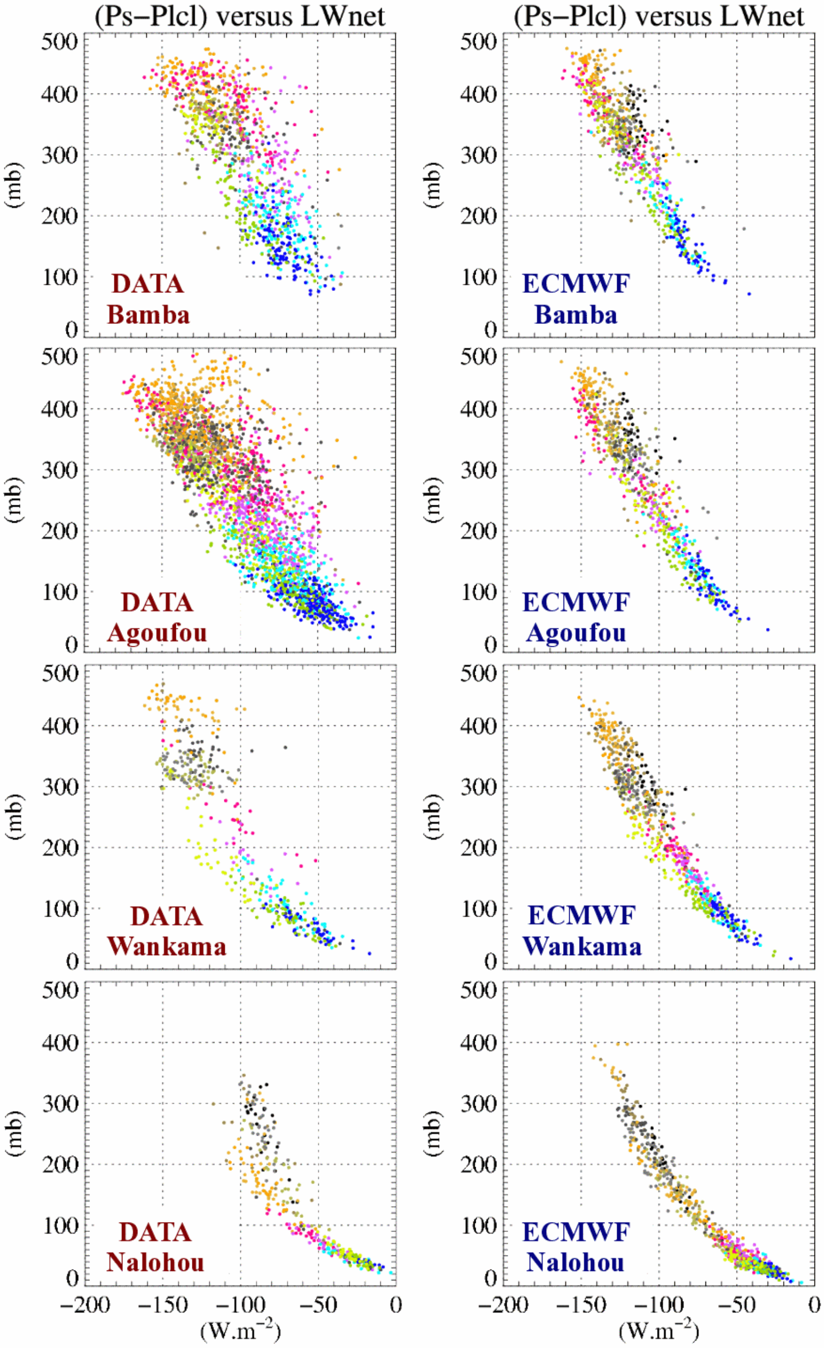

Figure B.1 *: Same as Fig. 2, i.e. scatter diagrams of daily-mean surface net longwave radiative flux versus lifting condensation level (P_s-P_{lcl}), for different sites (left panel) and for the ECMWF IFS model (right panel, using results for 2 years 2006 and 2007). The graphs are organized from North (top) to South (bottom). Note that much more data are used for the two northern sites, which probably partly accounts for the wider range of fluctuations.The colour code identifies months (same conventions as in Fig. 2).*

The ECMWF model compares reasonably well with observations at the four sites. For the two northern sites though, it tends to underestimate LW_{net}. More precisely, for a given (P_s-P_{lcl}), the values of LW_{net} coincide with the lower range of observed LW_{net} values. This could indicate that the amount of mineral aesosols is underestimated in the model (consistently with Guichard 2009).

Appendix C: Surface incoming longwave radiative flux versus precipitable water across sites

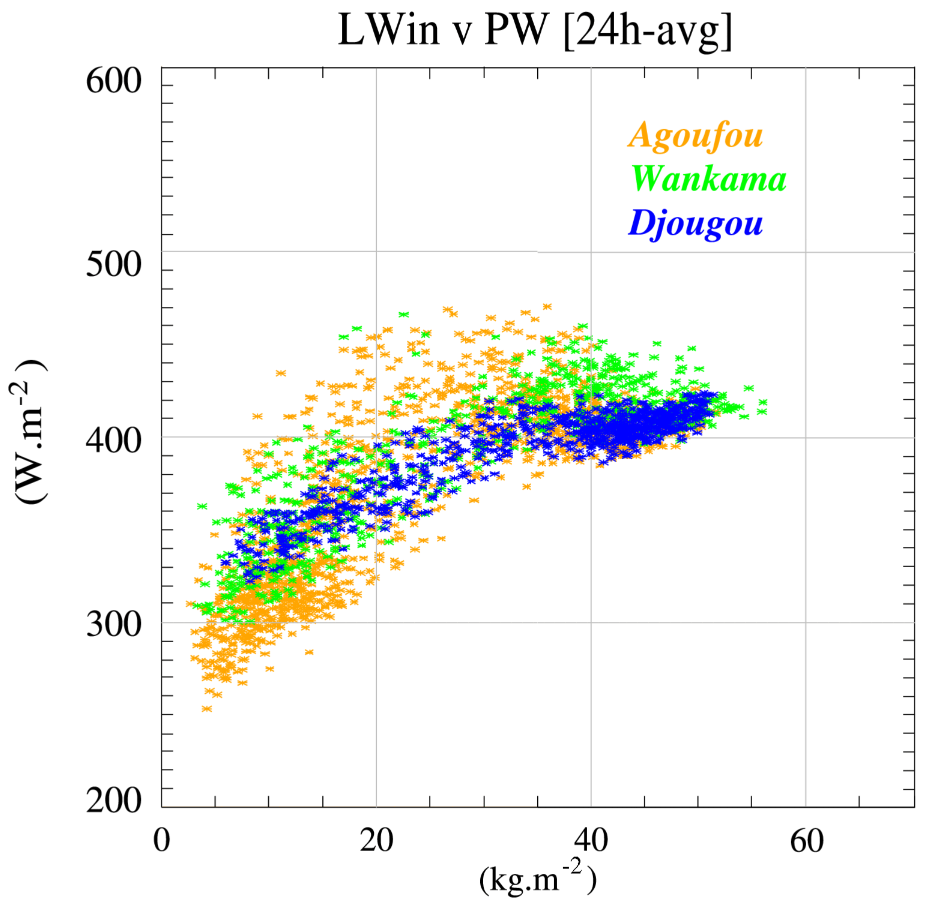

***Figure C1**: same as Fig. 3a (orange dots) but with the addition of data from Wankama in southern Sahel (green dots) and Djougou in the Soudanian zone (blue dots).*

Appendix D: DTR radiative scaling at different sites in observations and in the ECMWF model

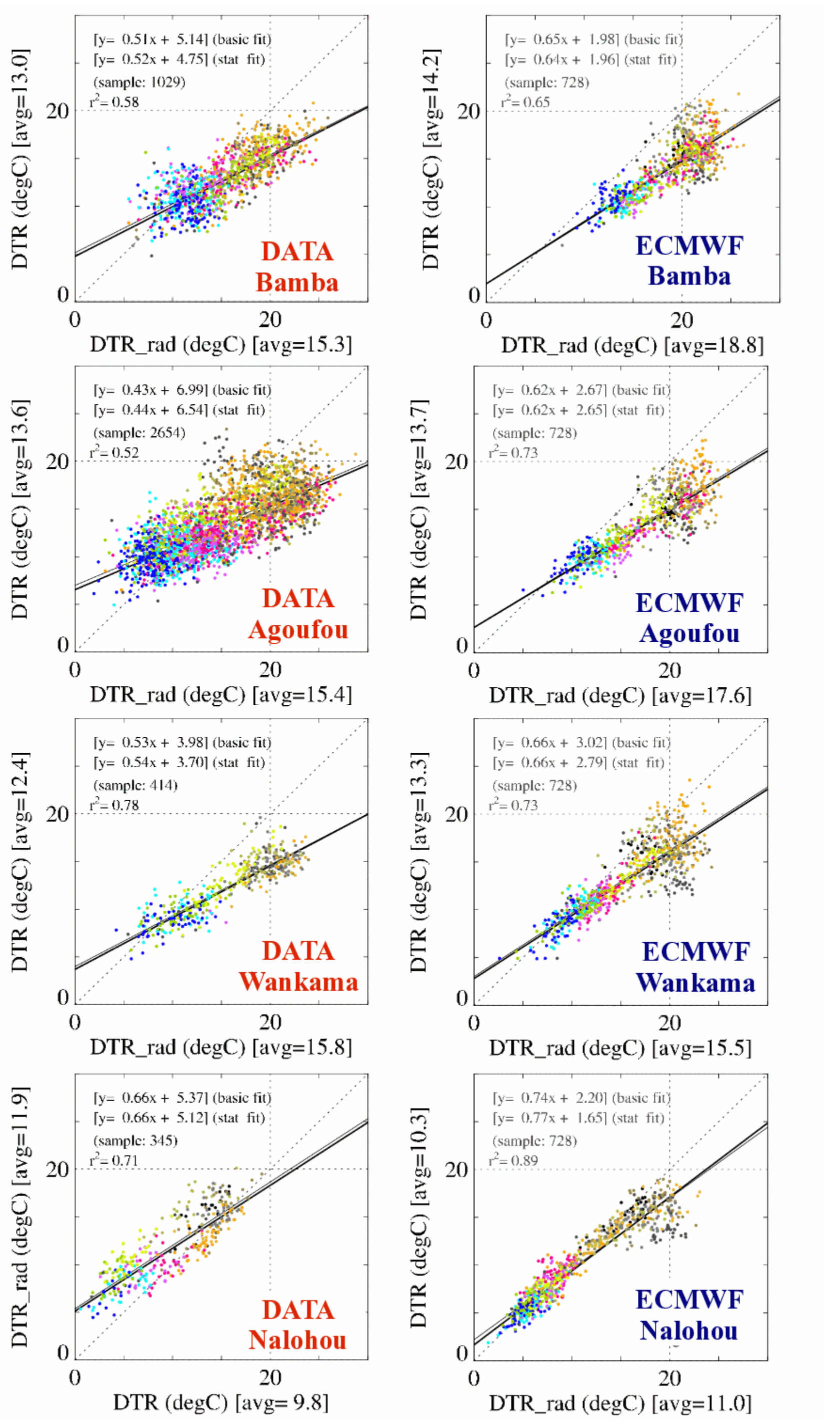

***Figure D1**: Scatter plots of daily-mean DTR versus DTR $_{RAD}$ at the different sites in observations (left panel) and in the ECMWF model (right panel), from Bamba (top) to Nalohou (bottom).The colour code identifies months (same conventions as in Fig. 2).*

Note that the slope of the fit increases from the northern to the southern sites. The ECMWF and observations are relatively close. However, the slope is generally higher in the ECMWF model than in observation, i.e. *DTR* is generally stronger and closer to *DTR* $_{RAD}$ in the model.

Appendix E: Inter-annual variability of the surface radiation budget during the monsoon

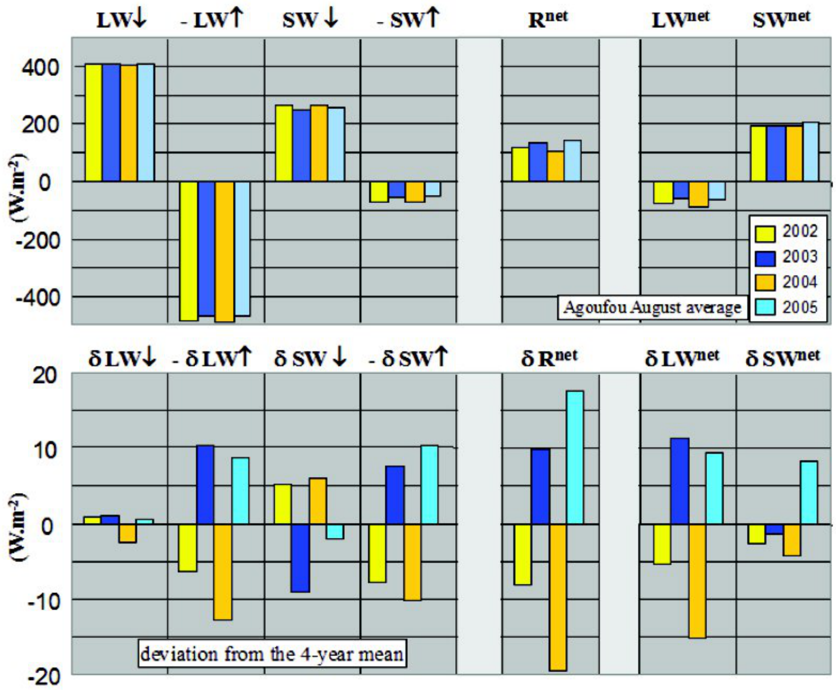

Figure E1: *surface radiative budget at Agoufou during the monsoon (August average), the different components (top panel) and their interannual fluctuations (bottom panel).*

Appendix F: evaluation of the annual cycle of surface radiation in CMIP5 models

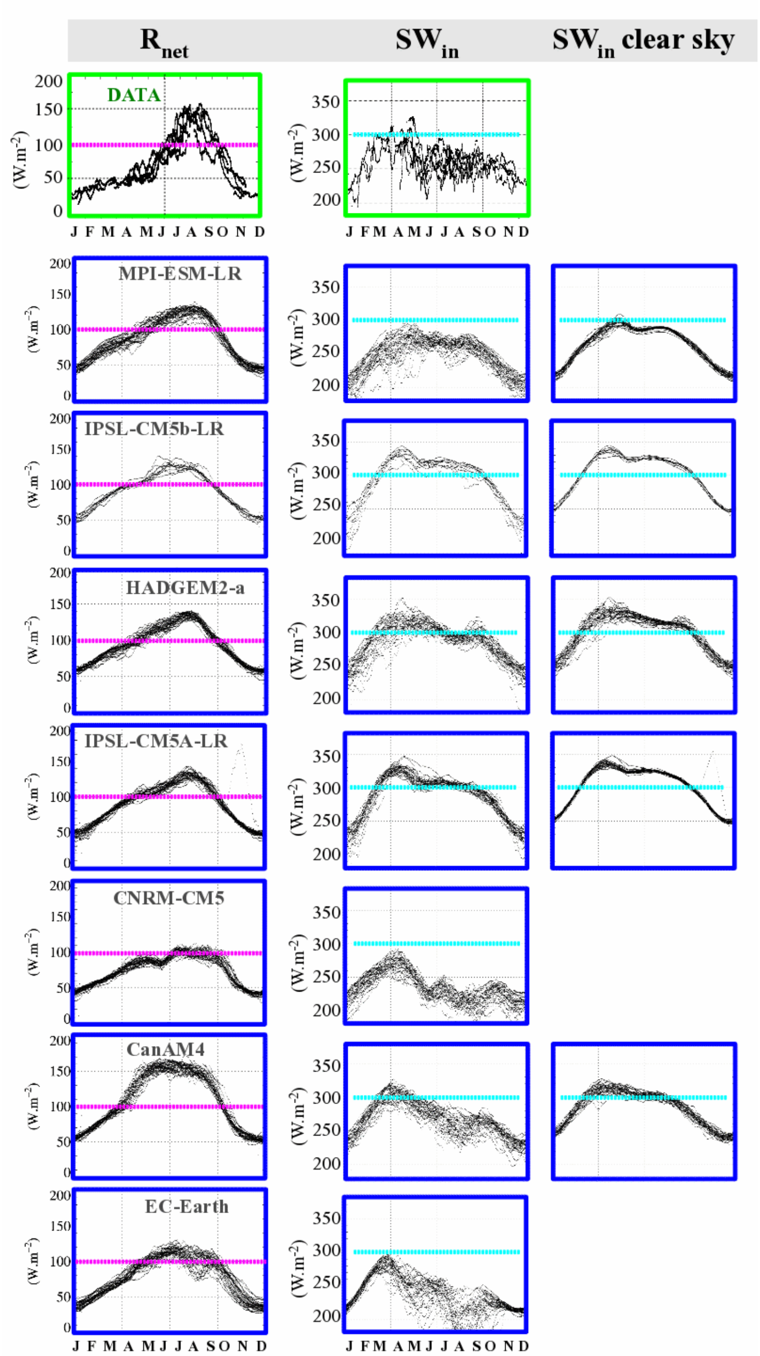

***Figure F1**: Annual cycle of surface net radiation (left column), incoming shortwave flux (middle column) and incoming clear sky shortwave flux (right column) in observation and CMIP5 amip simulations. The different curves correspond to different years (about 30 in simulations).*

Appendix G: Evaluation of the coupling between (P_s-P_{lcl}) and LW_{net} in CMP5 climate models

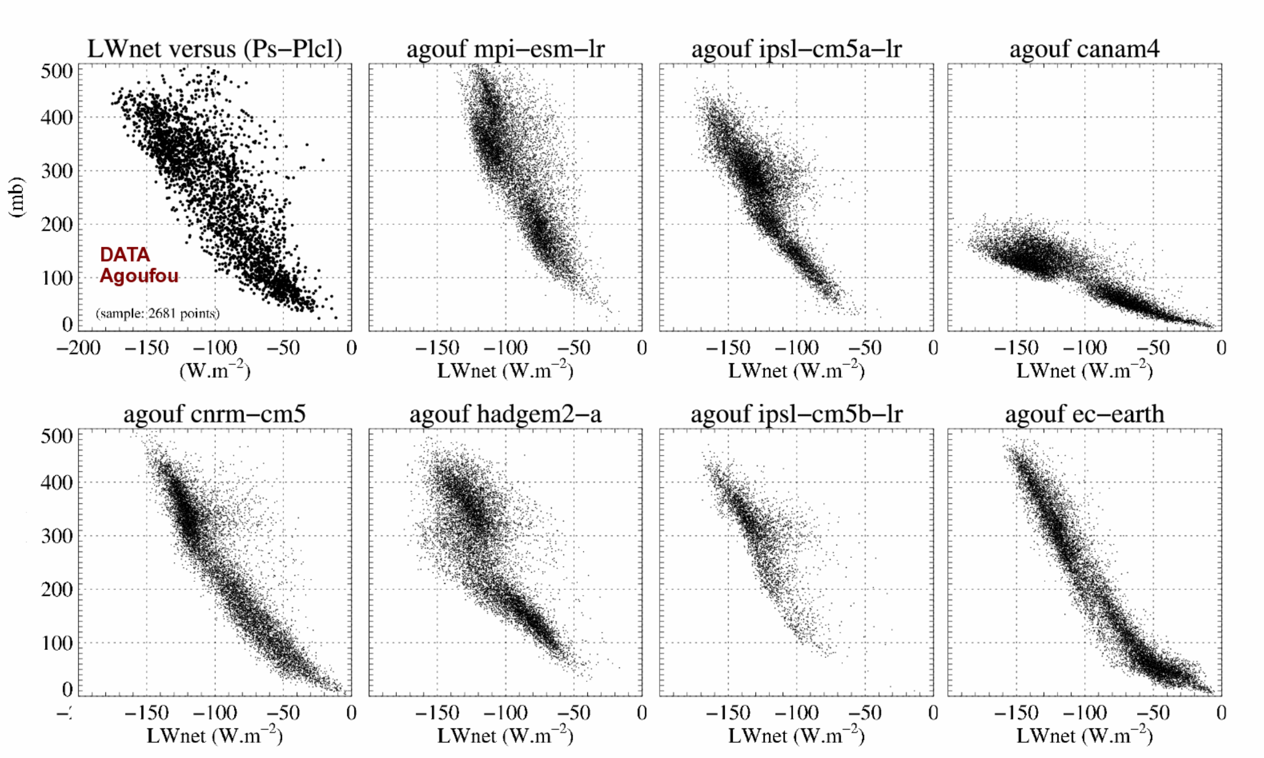

***Figure G1**: Scatter diagrams of daily-meanlifting condensation level versus surface net longwave flux.*

Appendix H: DTR radiative scaling at different sites in observations and climate models

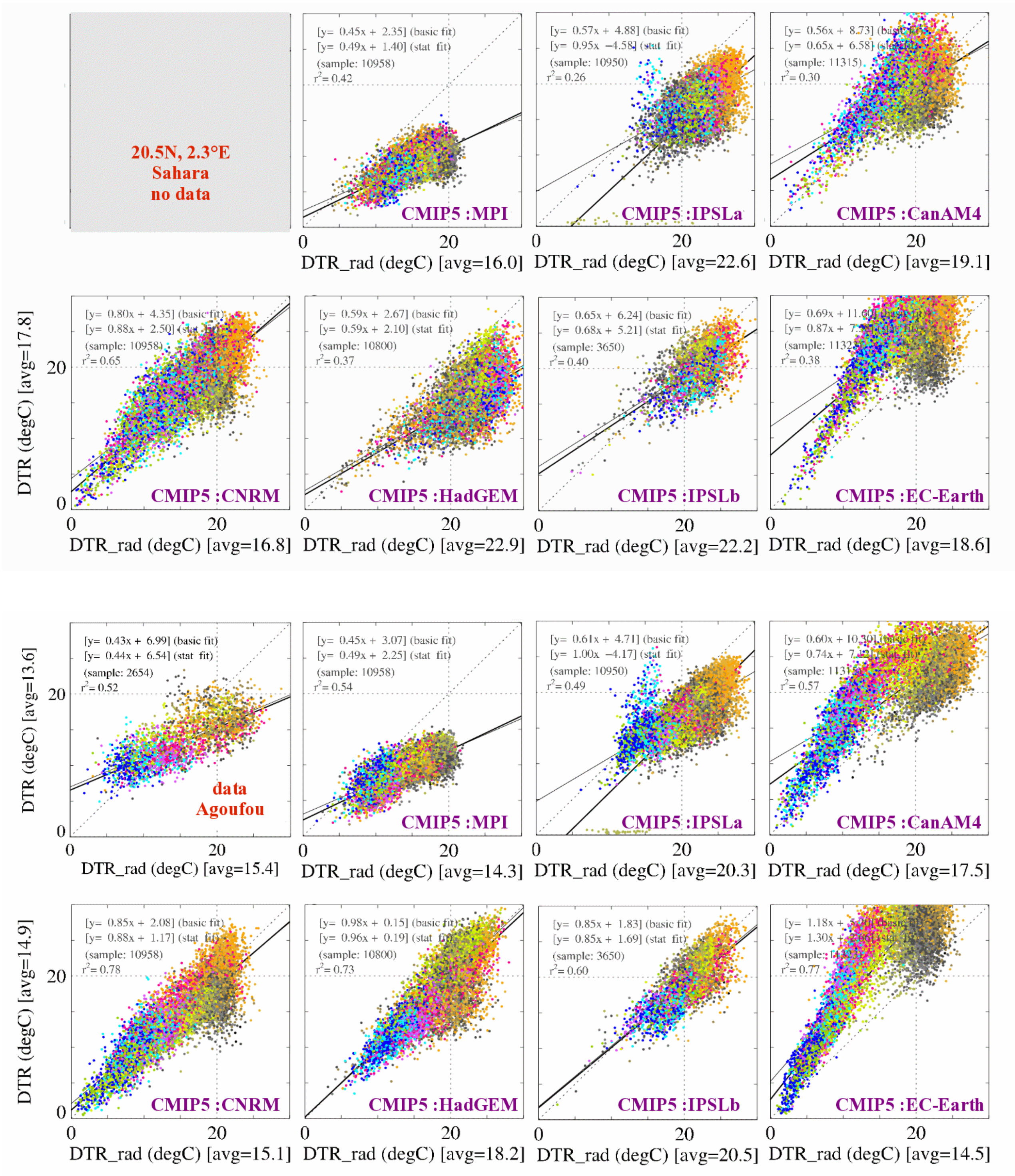

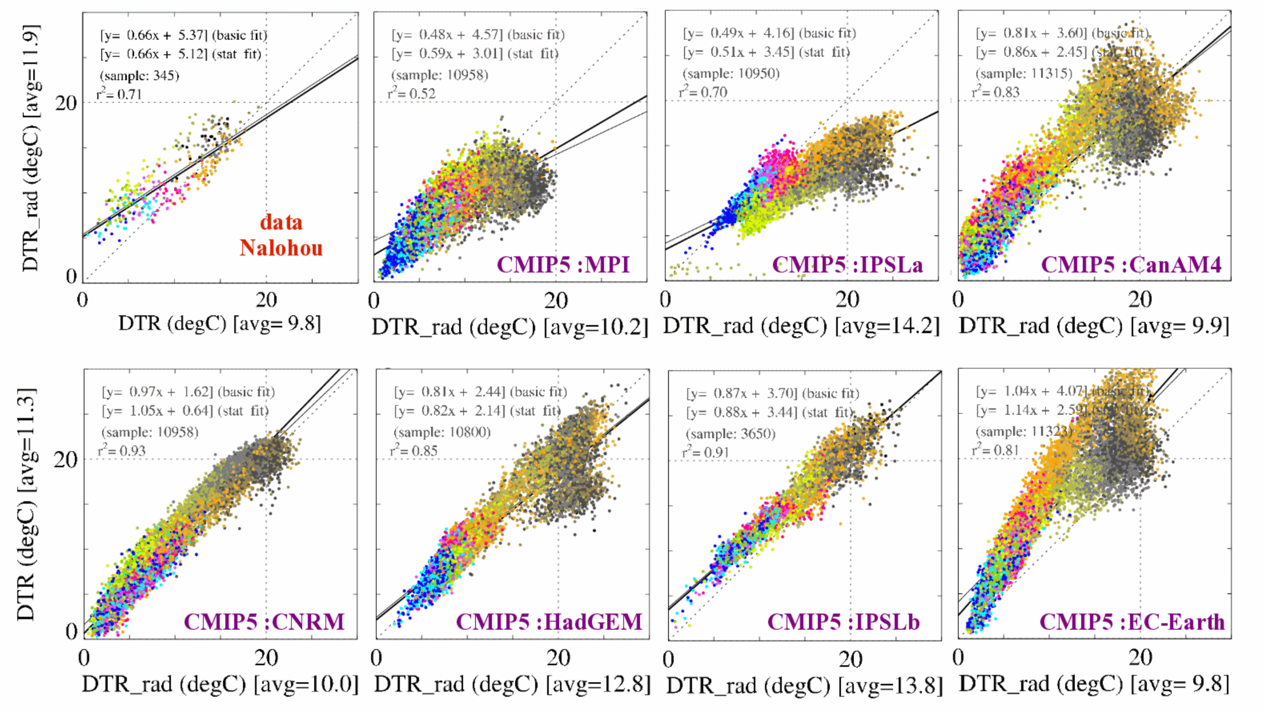

Figure H1: *Scatter plots of daily-mean DTR versus DTR $_{RAD}$ at different CMIP5 cfsites and in observations from the Sahara at [20.5°N, 2.3°E], to the Malian Gourma around [15°N,10°W], and finally the Ouémé basin in Benin around [10°N, 2°E]. The colour code identifies months (same conventions as in Fig. 2).*

Appendix I: Comparison of the scatter diagrams across sites in climate simulations

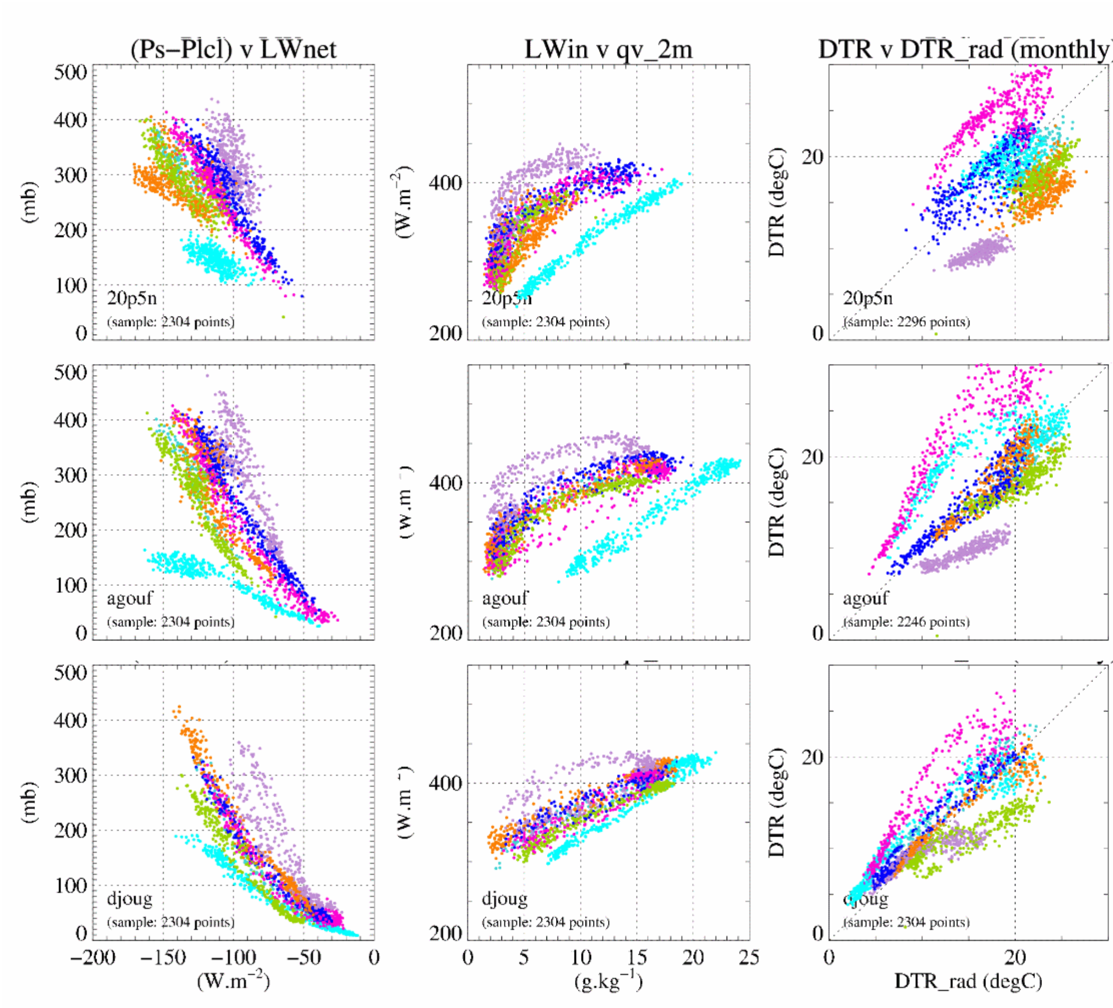

Figure I1: *Same as Fig. 8, left panel except for the cfSites at 2°E, 20.5°N (top), close to Agoufou, 1.5°W, 15.3°N (middle) and close to Djougou , 9.5°N, 2°E (bottom)*

References

Betts, A.K., 2004. Understanding hydrometeorology using global models. Bull. Amer. Meteor. Soc. 85, 1673–1688.

Betts, A. K., 2006: Radiative scaling of the nocturnal boundary layer and the diurnal temperature range, J. Geophys. Res., 111, D07105, doi:10.1029/2005JD006560.

Boone, A., P. de Rosnay, G. Balsamo, A. Beljaars, F. Chopin, B. Decharme, C. Delire, A. Ducharne, S. Gascoin, F. Guichard, Y. Gusev, P. Harris, L. Jarlan, L. Kergoat, E. Mougin, O. Nasonova, A. Norgaard, T. Orgeval, C. Ottlé, I. Poccard-Leclercq, J. Polcher, I. Sandholt, S. Saux-Picart, C. Taylor and Y. Xue, 2009 : The AMMA Land Surface Model Intercomparison Project (ALMIP), Bull. Atmos. Meteor. Soc. doi : 10.1175/2009BAMS2786.1

Bock, O., M.N. Bouin, E. Doerflinger, P. Collard, F. Masson, R. Meynadier, S. Nahmani, M. Koité, K. Gaptia Lawan Balawan, F. Didé, D. Ouedraogo, S. Pokperlaar, J.-B. Ngamini), J.P. Lafore, S. Janicot, F. Guichard and M. Nuret, 2008: The West African Monsoon observed with ground-based GPS receivers during AMMA, J. Geophys. Res., 113 (D21105). doi : 10.1029/2008JD010327

Bouniol, D., F. Couvreux, P.-H. Kamsu-Tamo, M. Leplay, F. Guichard, F. Fabot, E. O'Connor, 2012: Diurnal and seasonal cycles of cloud occurrences, types and radiative impact over West Africa. J. Appl. Met. Clim., 51, 534-553. doi: 10.1175/JAMC-D-11-051.1

Christensen, J. H. and F. Boberg, 2012: Temperature dependent climate projection deficiencies in CMIP5 models. Geophysis. Res. Lett., 39 (24), L24 705.

Dilley, A. C., and D. M. O'Brien, 1998: Estimating downward clear sky long-wave irradiance at the surface from screen temperature and precipitable water. Quart. J. Roy. Meteor. Soc., 124A, 1391–1401.

Frappart, F. P. Hiernaux, F. Guichard, E. Mougin, L. Kergoat, M. Arjounin, F. Lavenu, M. Koité, J.-E. Paturel and T. Lebel, 2009 : Rainfall regime over the Sahelian climate gradient in the Gourma, Mali, J. Hydrology, 375, 128-142 . doi : 10.1016/j.jhydrol.2009.03.007

Gounou, A., F. Guichard and F. Couvreux, 2012: Observations of Diurnal Cycles Over a West African Meridional Transect: Pre-Monsoon and Full-Monsoon Seasons. Boundary-Layer Meteorol., 144, 329-357. doi: 10.1007/s10546-012-9723-8

Guichard, F., L. Kergoat, E. Mougin, F. Timouk, F. Baup, P. Hiernaux and F. Lavenu , 2009: Surface thermodynamics and radiative budget in the Sahelian Gourma: seasonal and diurnal cycles, J. Hydrology, 375, 161-177. doi : 10.1016/j.jhydrol.2008.09.007

Guichard, F., 2009 : What can we learn from AMMA about physical processes and models? in ECMWF annual seminar, Seminar on Parametrization of subgrid physical processes, 1 - 4 September 2008, 283-308.

Guichard, F., L. Kergoat, C.M. Taylor, B. Cappelaere, M. Chong, J.-M. Cohard, F. Couvreux, C. Dione, A. Gounou, F. Lohou et M. Lothon, 2012: Interactions entre surface et convection au Sahel. La Météorologie, N° Special AMMA, 25-32. doi : 10.4267/2042/48129

Hourdin, F., I. Musat, F. Guichard, F. Favot, P. Marquet, A. Boone, J.-P. Lafore, J.-L. Redelsperger, P. Ruti, A. Dell' Aquila, T. Losada Doval, A. Khadre Traore and H. Gallee, 2009 : AMMA-Model Intercomparison Project, Bull. Amer. Meteor. Soc.. doi : 10.1175/2009BAMS2791.1

Jackson, L. S. and P. M. Forster, 2010: an empirical study of geographic and seasonal variations in diurnal temperature range. *J. Climate*, **23**, 3205–3221. doi: 10.1175/2010JCLI3215.1

Jin, M. and R. E. Dickinson, 2010: Land Surface Skin Temperature Climatology: Benefitting from the Strengths of Satellite Observations, Environ. Res. Lett. 5 044004

Karl, T.R., Kukla, G., Razuvayev, V.N., Changery, M.J., Quayle, R.G., Helm Jr., R.R., Easterling, D.R. and Fu, C.B. 1991: Global warming: evidence for asymmetric diurnal temperature change. Geophys. Res. Lett.,18, 2253-2256.

Kothe, S. and B. Ahrens, 2010: On the radiation budget in regional climate simulations for West Africa, J. Geophys. Res., 115, D23120. doi:10.1029/2010JD014331

Lohou, F., L. Kergoat, F. Guichard, A. Boone, B. Cappelaere, J.-M. Cohard, J. Demarty, S. Galle, M. Grippa, C. Peugeot, D. Ramier, C.M. Taylor, and F. Timouk, 2013: Surface response to rain events throughout the West African monsoon, Atmos. Chem. Phys. Discuss., 13, 18581-18620, doi:10.5194/acpd-13-18581-2013

Mougin, E. and Coauthors, 2009 : The AMMA-CATCH Gourma observatory site in Mali: Relating climatic variations to changes in vegetation, surface hydrology, fluxes and natural resources, J. Hydrology, 375, Pages 14-33. doi : 10.1016/j.jhydrol.2009.06.045

Nicholson, S., 2000: Land surface processes and Sahel climate. Rev. Geophys. 38, 117–139.

Prata, A. J., 1996: A new long-wave formula for estimating downward clear-sky radiation at the surface. Quart. J. Roy. Meteor. Soc., 122, 1127–1151

Roehrig R., D. Bouniol, F. Guichard, F. Hourdin and J-L Redelsperger: The present and future of the West African monsoon: a process-oriented assessment of CMIP5 simulations along the AMMA transect. J. Climate, doi: 10.1175/JCLI-D-12-00505.1

Samain O., L. Kergoat, P. Hiernaux, F. Guichard, E. Mougin, F. Timouk, and F. Lavenu, 2008: Analysis of the in-situ and MODIS albedo variability at multiple time scales in the Sahel, J. Geophys. Res., 113, D14119, doi:10.1029/2007JD009174

Sandu, I., A. Beljaars, P. Bechtold, T. Mauritsen, and G. Balsamo 2013, Why is it so difficult to represent stably stratified conditions in numerical weather prediction (NWP) models?, J. Adv. Model. Earth Syst., 5, doi:10.1002/jame.20013.

Slingo, A., H. E. White, N. A. Bharmal, and G. J. Robinson, 2009: Overview of observations from the RADAGAST experiment in Niamey, Niger: 2. Radiative fluxes and divergences, J. Geophys. Res., 114, D00E04, doi:10.1029/2008JD010497

Stein, T. H. M., Parker, D. J., Delanoë, J., Dixon, N. S., Hogan, R. J., Knippertz, P., Maidment, R. I. and Marsham, J. H., 2011: The vertical cloud structure of the West African monsoon: a 4 year climatology using CloudSat and CALIPSO. Journal of Geophysical Research, 116. D22205. ISSN 2156–2202

Stephens, G. L., M. Wild, P. W. Stackhouse, T. L'Ecuyer, S. Kato and D. S. Henderson, 2012: The global character of the flux of downward longwave radiation. J. Climate, 25, 2329–2340. doi: 10.1175/JCLI-D-11-00262.1